ARL 64-144
SEPTEMBER 1964

Aerospace Research Laboratories

MULTIAXIAL FAILURE OF VISCOELASTIC MATERIALS

A. R. ZAK
CALIFORNIA INSTITUTE OF TECHNOLOGY
PASADENA, CALIFORNIA

OFFICE OF AEROSPACE RESEARCH
United States Air Force

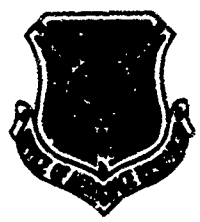

NOTICES

When Government drawings, specifications, or other data are used for any purpose other than in connection with a definitely related Government procurement operation, the United States Government thereby incurs no responsibility nor any obligation whatsoever; and the fact that the Government may have formulated, furnished, or in any way supplied the said drawings, specifications, or other data, is not to be regarded by implication or otherwise as in any manner licensing the holder or any other person or corporation, or conveying any rights or permission to manufacture, use, or sell any patented invention that may in any way be related thereto.

- - - - - - - - - -

Qualified requesters may obtain copies of this report from the Defense Documentation Center, (DDC), Cameron Station, Alexandria, Virginia.

- - - - - - - - - -

This report has been released to the Office of Technical Services, U. S. Department of Commerce, Washington 25, D. C. for sale to the general public.

- - - - - - - - - -

Copies of ARL Technical Documentary Reports should not be returned to Aerospace Research Laboratories unless return is required by security considerations, contractual obligations or notices on a specified document.

400 - November 1964 - 448-13-338

ARL 64-144

MULTIAXIAL FAILURE OF VISCOELASTIC MATERIALS

A. R. ZAK

CALIFORNIA INSTITUTE OF TECHNOLOGY
PASADENA, CALIFORNIA

SEPTEMBER 1964

Contract AF 33(616)-8399
Project 7063
Task 7063-02

AEROSPACE RESEARCH LABORATORIES
OFFICE OF AEROSPACE RESEARCH
UNITED STATES AIR FORCE
WRIGHT-PATTERSON AIR FORCE BASE, OHIO

FOREWORD

This is an interim report prepared by the Graduate Aeronautical Laboratories of the California Institute of Technology (GALCIT) for the Aerospace Research Laboratories, Office of Aerospace Research, United States Air Force under Contract No. AF 33(616)-8399, Task 7063-02, "Structures Research at Elevated Temperatures," of Project No. 7063, "Mechanics of Flight." This work is based upon analytical and experimental work accomplished from 1 January 1963 through 31 December 1963, under the cognizance of Mr. Charles A. Davies and Lt. W. J. Anderson, ARL Project Scientists.

It is a pleasure to acknowledge the assistance of Mr. L. W. Cronk and Mr. H. E. Ahlgren in the experimental program. The notes and data for this report are recorded in GALCIT File No. SM 64-6.

ABSTRACT

This report contains theoretical and experimental studies related to the failure phenomena in polymeric materials. In Section 1.0, first a review and a discussion is presented of the pertinent work which has been published in this area. Then, a new engineering failure theory is developed and described. This theory takes into consideration general, multiaxial viscoelastic loading conditions. The theory can be used to predict failure under multiaxial stress conditons if the uniaxial viscoelastic failure envelope is known.

In Section 2.0 a viscoelastic stress analysis of the poker-chip specimen is presented. This analysis is needed in order to evaluate the failure data from the triaxial poker-chip test.

In the experimental failure studies the Solithane 113 polymer material is being used. This material is being made and cured in the laboratory in a specially constructed facility. In Section 3.0 this facility and the manufacturing process are described in detail.

The Section 4.0 deals with the experimental program and the data obtained. Two types of tests are described; the uniaxial and the triaxial. The uniaxial test is conducted at various constant strain rates and temperatures. The purpose of this test is first to produce data for the viscoelastic characterization of the Solithane 113 material and secondly, to produce uniaxial failure data. The triaxial test uses the poker-chip specimen and its purpose is to generate failure data under triaxial stress conditions. These tests are also conducted at various strain rates and temperatures.

TABLE OF CONTENTS

1.0 FAILURE THEORY FOR POLYMERIC MATERIALS UNDER GENERAL MULTIAXIAL LOADING CONDITIONS

1.1 INTRODUCTION

Recently polymeric materials are finding an increasing use as structural components in various engineering areas, as, for example, a solid propellant fuel in the rocket industry. Although the primary role of these propellants is not structural, they nevertheless must withstand large loads. When a material is used in a structural member of a system it becomes necessary to speak about its structural integrity. Basically, the structural integrity analysis attempts to answer two questions: Are the deformations excessive, and are the components sufficiently strong? In order to answer these two questions it is first necessary to carry out a stress analysis for each component of the system. Once the stresses are known, the deflections and the deformations will also be known or can be calculated directly; but in order to answer the question whether the component will break, it is necessary to know also the failure criteria for the material. It is obvious from the above discussion that if polymeric materials are to be used for structural purposes it is necessary that one be able to conduct both a stress and a failure analysis.

In the last Interim Report, reference 1.1, a state-of-the-art discussion was presented of the failure in viscoelastic materials. The existing knowledge was reviewed and various possible failure criteria for multiaxial stress situations were discussed and compared to available data. In Section 5 of that report, certain important conclusions based on these discussions were drawn. Two of these conclusions were; one, that there has been little work in determining multiaxial failure criteria for viscoelastic materials as a function of strain rate and temperature and, two, that a multiaxial failure criterion has not yet been established for such materials. It was considered that this area of research was most important and work was therefore concentrated on this problem area during the last twelve months. The present report describes the results.

Polymeric materials are viscoelastic in nature, and therefore time enters explicitly into their stress analysis, thus making the analysis of polymer materials more difficult than the usual elastic one. In spite of this added difficulty the last few years have seen large advances in the methods of

---

Manuscript released by the author 18 May 1964 for publication as an ARL Technical Documentary Report.

viscoelastic stress analysis, see for example the state-of-the-art review in reference 1.9. It is now possible to analyze, for example, such situations as the stress in non-homogeneous materials, thermal stress problems, ablating boundary problems, discontinuous boundary-value problems, and wave propagation problems. Although there still remain many unresolved problems it is quite safe to say that, from the point of view of a practical engineer, the state-of-the art of viscoelastic stress analysis is well advanced. Unfortunately the same thing is not true regarding our knowledge of failure criteria, although from the point of view of structural integrity failure is fully as important as the stress analysis.

The reason for less work in the failure area is perhaps the fact that the failure mechanism in polymer materials is a very complex phenomena. For example, as we shall see later, the failure is very sensitive to time dependence of loading. In most practical situations the polymeric structural material will be subject to a triaxial stress state where the stresses will be different in different directions, and where also the time rates of change of various strain components will also be different and in general changing with time. In order to predict failure under such conditions it is necessary to have a failure criteria which takes into consideration these spatial and time variations. However, such failure criteria do not exist at present and this has motivated the development of the failure criterion to be described in the present report. The failure criterion will be developed from the engineering point of view as opposed to molecular or chemical derivation. Further, it will take into consideration general triaxial stress loading conditions as well as unequal and time variable rates of change for the different strain components.

There are two general ways that a rubbery polymeric material is observed to fail: one way is by tearing and the other is by global failure. Tearing occurs in situations where there is an obvious and well defined geometric discontinuity in the material, such as a crack or a void. Upon the application of load this imperfection grows with a resulting decrease in the amount of total material which can carry the applied load. This in turn will increase the local stresses and cause the discontunity to grow with an increasing rate, eventually leading to total failure. The various aspects of the tearing phenomena have been investigated quite extensively[1.1 to 1.9]*

* Superscripts refer to references at the end of the section.

In the global failure on the other hand no growth of any distinctive cracks or voids is observed before the fracture occurs - material seems to break suddenly. This does not, however, mean that there were no initial cracks or voids in specimens in which global failure is observed. On the contrary it is quite possible that such imperfections do actually exist in most polymeric materials but their growth is so small prior to the gross failure that it is not observed. However at the point of failure, stress and strain conditions exist which will promote very rapid and catastrophic growth of the imperfections leading to sudden total failure. If it is possible to define the conditions under which this sudden growth of small imperfections will occur we can speak of these conditions as being the global failure criterion. The use of a global criterion of failure in multiaxial stress conditions seems to be a most logical approach for predicting fracture since this type of situation has actually been observed in various tests[1.1] where no obvious initial imperfections were present. Therefore, the failure criterion which will be developed in the present report will be global, as distinct from local. However, before discussing this criterion it is instructive and appropriate to review previous investigations in this area.

Perhaps the best point of departure for this discussion is the experimental investigations of failure of viscoelastic materials. It is appropriate to mention at this point that nearly all the experimental data on viscoelastic failure has been obtained in uniaxial testing. One of the first comprehensive set of tests on amorphous polymers was carried out by Smith[1.10]. Working with a styrene butadiene rubber, usually referred to as SBR, he carried out uniaxial tensile tests at various temperaturs and various constant strain rates. It was found that the failure data obtained at different temperatures could be superimposed on one master curve by using the WLF[1.11] shift function. The data obtained in reference 1.10 for SBR rubber is not, in the quantitative sense, the same as has been obtained for other materials;[1.8, 1.12] however, other amorphous polymer materials have been observed to behave in a similar qualitative manner. Therefore, it is instructive to use this data for a more detailed discussion.

Figure 1.1 shows the reduced stress at break $S_m T_S/T$ as a function of the reduced strain rate of test Ra_T, where; T is the test temperature, T_S a standard or reference temperature, R the rate of strain, and a_T the WLF shift function. It can be seen that the stress at break decreases monotonically

with decreasing strain rate. In Figure 1.2 the ultimate strain γ_b is plotted against the reduced strain rate. It is easily seen that the strain at break possesses a definite maximum. For very large rates of testing the strain at break is relatively small and as the strain rate decreases the strain at break increases until about $Ra_T = 1$. Any further increase of rate after this point begins to reduce the ultimate strain until at very slow rates of testing the strain again becomes relatively small. The form of the plot in Figure 1.2 is sometimes referred to as the Smith curve. The data in Figures 1.1 and 1.2 are sometimes combined and the stress at break is plotted against the strain at break as shown in Figure 1.3. This type of a plot is usually referred to as a failure envelope. In further work on a slightly different type of SBR Smith and Stedry[1.13] reproduced, again experimentally, a portion of the failure envelope by testing for ultimate conditions in two different ways. Failure was obtained by using constant strain tests and constant strain rate tests. The results of these tests are reproduced in Figures 1.4 and 1.5 respectively. These figures were reproduced from reference 1.14. By comparing the curves in Figures 1.4 and 1.5 it can be seen that they are identical. This seems to imply that the failure envelope is independent of the types of tests which are used to obtain it. Although this conjecture is subject to further experimental verification it does seem to be reasonable for the SBR material and it has sometimes been taken for granted for other materials[1.15].

In contrast to the relatively large amount of uniaxial failure data there is very little data pertaining to global failure under multiaxial testing conditions. The only known published failure data for biaxial and triaxial tests is given in references (1.16), (1.17) and (1.29). The data in references (1.16) and (1.17) pertains to tests carried out under very slow, equilibrium load conditions. The data in reference (1.29) was obtained in triaxial tests on solid propellant specimens and it includes effects of variable temperature and strain rate. The lack of multiaxial viscoelastic failure data is mainly due to the difficulties in conducting such tests; nevertheless, experimental work in this area is urgently needed.

The theoretical analysis of failure in polymers has been primarily from the molecular point of view. In references 1.18 to 1.21 the uniaxial strength of a polymer was calculated without accounting for any viscoelastic effects. One of the first attempts to incorporate viscoelasticity in strength

calculations was by Bueche[1.22]. In his early theory Bueche evaluated the effect of strain energy in the stressed polymer on the rate of bond breaking. He then postulated that the total failure would occur when the rate of breaking of the bonds reached a certain value. This theory predicted a constant value of strain at failure no matter how fast the load was applied and therefore it did not agree with experimental observations. For this reason the theory was subsequently discarded. A few years later Bueche[1.23] again evolved a theory based on a molecular approach to predict the time to break a uniaxial polymer sample subject to a constant load. This theory was developed both with and without viscoelastic effects. There are no known experimental checks of those results. Knauss[1.8] also took the molecular approach in developing a failure theory. In this theory it was assumed that the material contained initial cavities whose growth under load was determined by a modified Griffith criterion. This theory is rather complex and necessitates experimental evaluation of certain parameters. The failure results obtained using this theory were compared with uniaxial constant strain rate test data. It was found that the ultimate strength as a function of strain rate was predicted by the theory. However, the ultimate strain, although it did possess a maximum, did not agree very well with the test data.

The most recent failure theory was developed by Bueche and Halpin[1.12]. Although the title of this theory implies a molecular approach there are really no molecular aspects used in the development. Furthermore the way the theory is developed, it applies only to a uniaxial creep situation under constant load. Nevertheless as it agrees closely with certain aspects of the experimental data it justifies a closer examination. In the conditions assumed in reference 1.12, a load is applied to a rubber specimen having a unit cross section. As a result the specimen will creep according to its creep compliance function D(t) which is related to the relative elongation λ and the nominal stress σ as follows:

$$D(t) = \frac{\lambda - \frac{1}{\lambda^2}}{1 - \frac{\lambda^2}{N}} \frac{1}{\sigma}$$

where $\lambda - 1/\lambda^2$ is a strain based on a statistical theory prediction and $1 - \lambda^2/N$ is an empirical correction for large elongations. The constant N is not known at

this point. The specimen is assumed to contain a crack, and at the tip of this crack the stress will be higher than the average stress by a factor of S. It is assumed that an element at the tip of the crack will break when the local relative elongation reaches a value of λ_{of} and this will happen at a time t' after the load is applied, therefore it follows that the local stress at break σ_{of} is

$$\sigma_{of} = S\sigma = \frac{\lambda_{of} - \frac{1}{\lambda_{of}^2}}{1 - \frac{\lambda_{of}^2}{N}} \cdot \frac{1}{D(t')} = \frac{SK}{D(t')}$$

where K is a constant since λ_{of} is assumed to be a constant. It is now assumed that when the first filament at the crack tip breaks the second filament will break after an additional time t' and so on. The whole specimen is assumed to fail when the tear propagates through q such filaments, therefore the time to break is $t_b = qt'$. Therefore the final relative elongation of the whole specimen at break λ_b is given by

$$\frac{\lambda_b - \frac{1}{\lambda_b^2}}{1 - \frac{\lambda_b^2}{N}} = D(t_b)\,\sigma = D(t_b)\,\frac{K}{D\left(\frac{t_b}{q}\right)}$$

and the ultimate stress is given by

$$\sigma_b = \frac{K}{D\left(\frac{t_b}{q}\right)}$$

It can be observed from the above expressions that the ultimate elongation can be obtained if the creep compliance, time to break and, the three constants q, K and N are known. In reference 1.12 the value of the constant q was estimated to be 10^4 and it can therefore be seen that the ratio $D(t_b)/D(t_b/q)$ would possess a maximum value somewhere between small and long times to break. It follows that λ_b would also possess a maximum and this is in accordance with previously discussed experimental observations. This fact is used in reference 1.12 to justify this theory. The two remaining unknown constants K and N are calculated by using the maximum point on the experi-

mental failure envelope and equating the stress and the ultimate extension to their theoretical values as calculated from the above expressions.

Certain immediate comments can be made about this approach. First the rupture propagation does seem to be oversimplified. For example, it is not at all obvious why the different elements should break at equal time intervals. On the contrary it can easily be argued that the rate would increase as the creep progresses. Secondly, it is not clear why a constant strain criterion for the rupture at the crack tip should be valid, this could very well be a function of the rate of extension which in turn is a function of the applied load. Since a large amount of experimental data is needed in order to evaluate certain unknown coefficients in this theory the usefulness of this approach would depend on whether it could be used to predict failure under different loading conditions. In order to do this it seems that more information should be obtained regarding rate of fracture at the crack tip and in particular how it depends on variable strains and stresses at the crack tip. A more detailed analysis of the crack propagation conditions, for example such as presented in reference 1.7, may be useful.

From the above discussion certain definite conclusions can be drawn. First, the experimental data on viscoelastic failure has been obtained for uniaxial stress conditions only and data for multiaxial loadings is needed. Secondly, the theoretical treatments of viscoelastic failure have also been limited to uniaxial situations. Finally agreement with experimental data, for most of these theories and especially the molecular approaches has not been good. This does not indicate that the molecular failure theories have been useless. On the contrary, the final basic explanation and understanding of the failure phenomena can only be achieved on molecular level. However, this does indicate that at the present time the state-of-the-art does necessitate many unknown averaging processes in going from the single molecular chain to network and then to macroscopic behavior. These approximations can lead to incorrect results. Therefore more molecular knowledge has to be gathered before this approach can be useful in producing a workable engineering failure criteria. In the meantime the structural analyst does need a criterion which he can use for multiaxial viscoelastic situations. It is thought therefore that a temporary criterion can be obtained from a macroscopic point of view based on existing experimental knowledge and observations. In this report we shall proceed to develop such a criterion.

1.2 FAILURE CRITERION

1.2.1 Uniaxial Stress Case

We refer to the experimental results for SBR shown in Figure 1.1 which illustrate the large effect of strain rate upon the ultimate stress in uniaxial tension. The relatively large strength at high rates and the relatively low strength at low rates can be explained on the global scale as follows. During an unstressed state the polymer chains are twisted around each other and are connected at points by chemical cross-linking bonds. When a load is applied it will deform the material which will cause stretching and untwisting of the polymer chains. The untwisting of the polymer chains is accompanied by internal frictional forces which give rise to viscoelastic nature of the material. The load can be transmitted from one portion of the material to another in two ways. First,it is transmitted by chemical bonds at the point of the cross linking of the chains and secondly, it is transmitted by the frictional forces between the chains.

Considering now an internal plane in the material,the loads across this plane will be divided among a certain number of polymer chains which are oriented approximately in the direction of the load. At any instant this number of load-carrying chains will depend on the particular network configuration, i.e., cross-link density and distribution, and on the amount of active entanglements between the chains. The term "active entanglements" is used here to denote frictional contact points between the chains. Therefore for a particular polymer the number of load-carrying chains will be a function of the amount of active entanglements and this in turn will depend on the "state of relaxation" of the material at any particular time. The term relaxation is used here in a broad sense to denote how far the material is from rubbery equilibrium. We shall subsequently define this quantity in a mathematical form. It should be mentioned that the basic idea involving the change of the number of load-carrying chains with state of relaxation is not new and has been used by Bueche[1.24].

Consider now a uniaxial specimen which at a particular time, is subject to a tensile load σ. No restrictions are placed on the way in which this load is reached. At the same time it is assumed that over the cross section of the specimen there are $\underline{n}$ polymer chains over which the load is distributed. The number $\underline{n}$ will, as discussed above, be dependent on stress and strain conditions in the specimen. The average force, f, in each load-carrying chain is therefore given by

$$f = \frac{\sigma}{n} \qquad (1.2.1)$$

It is now necessary to relate n to the stress and strain conditions in the specimen or, as indicated above, to the "state of relaxation." This relationship will now be developed.

At the instant that the tensile load on the specimen has the value σ the longitudinal strain is ϵ . The longitudinal and transverse relative extensions are denoted by λ and λ_t respectively. The relation between the strain and the extension ratio will be developed later. Assuming that the original unstrained cross section of the specimen is unity the true stress at a particular time will be σ/λ_t^2 . A point corresponding to this stress and the strain ϵ is shown on the stress-strain plane in Figure 1.6. Shown in this figure are also two straight lines corresponding to the glassy and the rubbery response of the material. The question now is: what is the "state of relaxation" of the point given by σ/λ_t^2 , ϵ coordinates. One way that this state can be measured is if we imagine that at any instant the stress σ/λ_t^2 is frozen and we observe how far the specimen must extend in order to achieve rubbery equilibrium. Therefore the "state of relaxation" can be measured by the relative distance of the point in Figure 1.6 from the glassy and rubbery states where the distance is measured along a constant stress line, this line is shown as a horizontal dotted line. Therefore the relative distance from the rubbery, or glassy, state can be expressed by the ratio

$$\frac{\epsilon - \epsilon_G}{\epsilon_R - \epsilon_G} = \frac{\epsilon - D_G \frac{\sigma}{\lambda_t^2}}{D_R \frac{\sigma}{\lambda_t^2} - D_G \frac{\sigma}{\lambda_t^2}} = \frac{\frac{\epsilon \lambda_t^2}{\sigma} - D_G}{D_R - D_G} \qquad (1.2.2)$$

or since for practical cases $D_G << D_R$ and also $D_G << \frac{\epsilon \lambda_t^2}{\sigma}$, we can write

$$\frac{\frac{\epsilon \lambda_t^2}{\sigma} - D_G}{D_R - D_G} = \frac{\epsilon \lambda_t^2}{D_R \sigma}$$

where D_G and D_R are the glassy and the rubbery creep compliances respectively.

Referring to equation (1. 2. 1) we can, therefore, write the number n as some function of the ratio in equation (1. 2. 2)

$$n = g\left(\frac{\epsilon \lambda^2_t}{\sigma D_R}\right) \tag{1. 2. 3}$$

The exact form of this function is at present unknown; however if the above assumptions are correct we know that g must be a monotically decreasing function of $\epsilon \lambda^2_t / \sigma$. We shall subsequently see, by analyzing available experimental failure data and determining g, that this indeed does happen.

A failure criterion is now postulated. We say that fracture of the specimen will occur when the average tensile force f in the load-carrying polymer chains reaches some critical value f_b. Therefore in mathematical form the failure criterion is

$$f_b = \frac{\sigma_b}{g\left(\frac{\epsilon_b \lambda^2_{tb}}{\sigma_b D_R}\right)} \tag{1. 2. 4}$$

or

$$f_b g\left(\frac{\epsilon_b D_R \lambda^2_{tb}}{\sigma_b D_R}\right) = \sigma_b \tag{1. 2. 5}$$

where the subscript b is used to indicate the critical, or breaking, values of the various quantities. It is appropriate to point out at this point that the failure criterion represented by equation (1. 2. 5) gives an explicit relation between σ_b and ϵ_b which does not depend on the manner in which these conditions were reached. Therefore in this respect the criterion agrees with the experimental observations on SBR by Smith and Stedry[1. 14] that the failure envelope is independent of the test conditions.

In order that the criterion (1. 2. 5) can be applied for any particular material it is necessary that the function $f_b g$ be known for this material. A theoretical way of determining this function, if it is indeed possible, would have to be done on the molecular level. In view of the previous statements

regarding molecular network theories we would expect that such a theoretical calculation would involve a rather complex analysis. We therefore will not attempt in the present approach to calculate this function but rather we shall adopt the following attitude. If this function can be determined experimentally from uniaxial tests and if this failure criterion can be extended to multiaxial situations we shall be able to predict failure under the latter conditions from uniaxial data. As stated previously the function g must be a monotonically decreasing function of the variable $\epsilon_b \lambda^2_{tb}/\sigma_b$ if the present theory is correct. We, therefore, have proceeded to assume a number of different expressions for the product $f_b g$ which satisfy this condition. At first a most simple form was assumed and the results compared with uniaxial failure data of references 1.10 and 1.12. The form assumed was

$$f_b g = A\left(1 - K \frac{\epsilon_b \lambda^2_{tb}}{\sigma_b}\right) \tag{1.2.6}$$

In order to compare the above criterion with the uniaxial data it was assumed that the material in question was incompressible and therefore $\lambda_t = 1/\sqrt{\lambda}$. Also it was necessary to relate the strain ϵ to the longitudinal extension λ. For small extensions the relation between ϵ and λ is simply

$$\epsilon = \lambda - 1 \tag{1.2.7}$$

however for large extensions the above relation is no longer true since nonlinear effects are important.

It is necessary therefore to develop at this point certain ideas regarding large extensions in viscoelastic materials. In general nonlinear uniaxial situations, the true stress in the material $\sigma\lambda$ will be related to the longitudinal extension λ and time t through some function as follows

$$\sigma = F(\lambda, t) \tag{1.2.8}$$

where F would, in general be nonlinear in λ and t. It is to be noted that function F used here is only in symbolic form and it is not limited to algebraic functions but can also contain derivatives and integrals. For certain materials and under certain loading conditions it has been shown experimentally that the large strain relation, represented by equation (1.2.8), can assume reasonably simple form.

Guth, Wack and Anthony[1.25] showed that for certain polymers under stress relaxation conditions the function F in equation (1.2.8) can be separated into two portions, one portion being a function of the extension ratio λ only and the other only a function of time t. Therefore for such materials in stress relaxation condition

$$\sigma(\lambda, t) = \Gamma(\lambda)\, E(t) \tag{1.2.9}$$

where $\Gamma(\lambda)$ is some function of λ which approaches $\lambda - 1$ when λ approaches unity, and E(t) is the relaxation modulus. Equation (1.2.9) implies that in stress relaxation the material can be considered to be pseudo-linear if a measure of strain other than $\lambda - 1$ is used. Similar results were obtained by Leaderman[1.26] when he showed that linear superposition relations were valid for large extensions. Using creep and creep recovery data he showed that polyvinyl chloride material obeyed a linear superposition law if the strain was defined as some empirical function of the extension ratio.

Smith[1.27] obtained similar results for the behavior of SBR under constant strain rate conditions. He showed that the stress could be expressed as a separable function of extension ratio λ and time t. Therefore this material, under this loading, can be considered as linear if the strain is defined as some particular function of λ. The relationship defining this function was obtained from experimental data and presented in curve form. It was also found that for a large range of the test conditions this relationship could be expressed in an analytical form by the empirical Martin-Roth-Stiehler[1.28] equation

$$\epsilon = \frac{\lambda - 1}{\lambda}\, e^{-.49(\lambda - \frac{1}{\lambda})} \tag{1.2.10}$$

where the corresponding stress is the true stress given by $\sigma\lambda$. It is clear from the above discussion that certain polymeric materials will possess linear superposition even under large uniaxial extensions.

Therefore, in order to compare the failure criterion predicted by equation (1.2.6) with available experimental data we shall assume that such a linear superposition is valid and that the relationship between the strain and extension is given by the empirical formula in equation (1.2.10). It should be noted here that such a linear superposition was really implied earlier when

it was taken for granted that the glassy and the rubbery compliances, D_G and D_R, were not functions of the extension ratio. If the linear superposition should prove to be not valid for any material, then these quantities would depend on λ. The use of the empirical formula (1.2.10) is chosen here for convenience, and also since no better expressions exists at present for the materials which will be discussed. If it proves later that an alternate expression is more suitable for these materials, the general conclusions which will be drawn here will not be altered.

The failure criterion (1.2.6) was compared with experimental results for SBR from reference 1.10, and the results for SBR and for ethylene propylene rubber (EPR) from reference 1.12. The two unknown parameters A and K in equation (1.2.6) were evaluated by matching the theoretical curve with experimental data at two points. It was found in each case that, although equation (1.2.6) predicts a maximum in the failure envelope, the shape of the envelope is not predicted well. For example if the parameters A and K were chosen so that the theory and experiment agreed near the maximum point then the stress range of the predicted envelope was too small. If, however agreement was obtained at the two extreme ends of the envelope then the agreement was not good near the maximum point. Expression (1.2.6) was, therefore, discarded. In order to obtain a better expression the form of the function $f_b g$ was evaluated in a curve form from the experimental data for SBR[1.10] shown in Figure 1.3. It was found that when log $f_b g$ was plotted against $\epsilon_b/\sigma_b\lambda$ a nearly straight line was obtained. This indicated that $f_b g$ should be given by the expression

$$f_b g = A\ 10^{-k\frac{\epsilon_b}{\sigma_b \lambda_b}} \qquad (1.2.11)$$

Therefore from equation (1.2.5) the failure criterion has the form

$$\sigma_b = A\ 10^{-k\frac{\epsilon_b}{\sigma_b \lambda_b}} \qquad (1.2.12)$$

Choosing a set of values for the parameters A and K the criterion (1.2.12) was compared to the experimental data of references 1.10 and 1.12. In Figure 1.7 the failure envelope for SBR, which has already been shown in Figure 1.3, is compared with the theoretical prediction of equation (1.2.12).

The parameters A and K were chosen by comparing (1.2.12) to the experimentally predicted form of $f_b g$ as discussed above. Therefore a reasonably good agreement is really forced and is therefore expected. Of more interest is the comparison of the criterion (1.2.12) to the data in reference 1.12. In Figure 1.8 this comparison is shown for SBR, also shown are the failure envelopes predicted by the theory of reference 1.12. It can be observed that the present theory does agree with the experimental data as well as, if not better, than the theory of reference 1.12. The parameters A and K were chosen by trial and error method and the agreement between the theory and experiment could perhaps be even further improved by a more refined choice. In Figure 1.9 the theory is compared to the test data on EPR again taken from reference 1.12. The envelopes obtained from the theory of reference 1.12 are also shown. It can be observed that again a reasonable agreement between the present theory and the observed failure data is obtained however, this agreement is not as good as in Figures 1.7 and 1.8 for the two different SBR materials. This could perhaps be due to the fact that in Figure 1.9 there is a reasonably large scatter in the experimental data and also the experimental failure envelope does seem to have a rather abrupt change of shape near the point $\lambda_b = 5.8$. Again the parameters A and K were chosen by trial and error method in order to achieve the agreement shown in Figure 1.9. It should be noted that the stress at break σ_b which is used in Figures 1.7 to 1.9 is the temperature reduced stress.

The main point which has to be made from the above comparisons is that the present theory does indeed predict a maximum in the failure envelope for uniaxial testing. Also, the agreement between the theoretical and experimental predictions can be improved even further by assuming other more complex functions for $f_b g$ in equation (1.2.11).

1.2.2 Multiaxial Stress Case

The failure criterion developed in the last section will now be extended to the multiaxial situations. For the purpose of developing certain necessary ideas we introduce into the stressed material an orthogonal cartesian coordinate system where the three different directions are denoted by 1, 2 and 3. This system is illustrated in Figure 1.10. Consider now a rectangular cube of the material, shown in Figure 1.10, whose faces are perpendicular to the three axes. The normal nominal stresses acting on the

faces of this cube are denoted by σ_1, σ_2, and σ_3, and the relative extensions along these three directions are denoted by λ_1, λ_2, and λ_3. It is not implied that these directions are necessarily principal directions. The stresses and the extensions are the instantaneous values and are time dependent according to the viscoelasticity of the material.

Proceeding now as in the case of the uniaxial stress situation, we calculate the average tensile stress in the load-carrying polymer chains at the different faces of the cube of the material shown in Figure 1.10. For the purpose of the subsequent discussion we choose the face which is perpendicular to axis 1. Therefore, if we denote the instantaneous number of the load carrying polymer chains across this face by the number n_1 we have

$$f_1 = \frac{\sigma_1}{n_1} \tag{1.2.13}$$

where f_1 is the average normal component of the force in each polymer chain. It is obvious that the shear forces on this plane will not contribute to the normal component. However, if there is a shear stress, it will be manifested as tensile or compressive stress along some other direction in the material. The effect of this will be taken into account since the orientation of the coordinate system shown in Figure 1.10 is arbitrary and it will be allowed to rotate in all possible directions in the material.

The problem is now to evaluate n_1. As in the case of the uniaxial stress, the effective number of the load-carrying chains will be a function of the "state of relaxation" of the material. Since the "state of relaxation" is the measure of the frictional forces in the material and the latter can be different in the different directions, therefore, the "state of relaxation" has to be considered as a directional property. For given stress histories along the axes 2 and 3 and for a given instantaneous stress σ_1 the instantaneous strain ϵ_1 will depend on the number of the frictional forces in the direction 1. Therefore, the strain ϵ_1 can be taken to be a measure of the "state of relaxation" in the direction 1. However, in order that we may use this, we must compare ϵ_1 to some reference states. For this we again choose the glassy and the rubbery responses which are defined as follows.

At any given time and for any given stress history in the directions 2 and 3 the maximum number of frictional forces in the direction 1 would be obtained if the stress σ_1 was applied instantaneously. This we refer to as a glassy response and denote this by ϵ_{G_1}. Similarly, the least number of frictional forces in direction 1 would occur if the load σ_1 had been applied for a long time so that it can be considered to be constant with time. Under these conditions the viscoelastic effects due to σ_1 have disappeared and we refer to this state as rubbery response and denote it by ϵ_{R_1}. We can express these quantities in a methematical form. For a general homogeneous and isotropic material the strain ϵ_1 can be written in the integral form.

$$\epsilon_1 = \int_0^t D_1(t-\tau) \frac{\partial \sigma_1}{\partial \tau} \, d\tau - \int_0^t D_2(t-\tau) \left[\frac{\partial \sigma_2}{\partial \tau} + \frac{\partial \sigma_3}{\partial \tau} \right] d\tau \qquad (1.2.14)$$

In equation (1.2.14) the two functions $D_1(t)$ and $D_2(t)$ are the time dependent viscoelastic properties of material. The glassy response ϵ_{G_1} and the rubbery response ϵ_{R_1}, as defined above, can be obtained from equation (1.2.14)

$$\epsilon_{G_1} = D_{G_1} \sigma_1 - \int_0^t D_2(t-\tau) \left[\frac{\partial \sigma_2}{\partial \tau} + \frac{\partial \sigma_3}{\partial \tau} \right] d\tau \qquad (1.2.15)$$

$$\epsilon_{R_1} = D_{R_1} \sigma_1 - \int_0^t D_2(t-\tau) \left[\frac{\partial \sigma_2}{\partial \tau} + \frac{\partial \sigma_3}{\partial \tau} \right] d\tau \qquad (1.2.16)$$

where D_{G_1} is the short time, or the glassy, value of $D_1(t)$ and D_{R_1} is long time, or the rubbery, value of the same function. Proceeding as in the case of the uniaxial stress we take the following ratio as the measure of the "state of relaxation" of the material in the direction 1

$$\frac{\epsilon_1 - \epsilon_{G_1}}{\epsilon_{R_1} - \epsilon_{G_1}} = \frac{\int_0^t D_1(t-\tau) \frac{\partial \sigma_1}{\partial \tau} - D_{G_1} \sigma_1}{D_{R_1} \sigma_1 - D_{G_1} \sigma_1} \qquad (1.2.17)$$

where in the above expression we have used equations (1.2.14) to (1.2.16) to express the strains as a function of the stress. As previously, we are again justified in making the assumption that $D_{R_1} >> D_{G_1}$ and therefore we can write

$$\frac{\epsilon_1 - \epsilon_{G_1}}{\epsilon_{R_1} - \epsilon_{G_1}} \doteq \frac{\int_0^t D_1(t-\tau) \frac{\partial \sigma_1}{\partial \tau} - D_{G_1} \sigma_1}{D_{R_1} \sigma_1} \tag{1.2.18}$$

We have not, as in the case of the uniaxial stress, made the assumption that the glassy response ϵ_{G_1} is small compared with ϵ_1 since in certain multiaxial loading conditions this would not be valid.

The number of the loading-carrying polymer chains in the direction 1 will be some function of the ratio in equation (1.2.18). We, therefore, assume here that since the network behavior is basically similar in the uniaxial and multiaxial loading situations the number of polymer chains n_1 will be equal to the g function given in equation (1.2.3) where the function variable is now the ratio in equation (1.2.18). This implies that n_1 is known if g has been determined from the uniaxial case. We can, therefore, write

$$n_1 = g\left(\frac{\int_0^t D_1(t-\tau) \frac{\partial \sigma_1}{\partial \tau} - D_{G_1} \sigma_1}{D_{R_1} \sigma_1}\right) \tag{1.2.19}$$

The normal component of the force f_1, in equation (1.2.13), can now be calculated.

Our aim in the present theory will be to relate the failure conditions under multiaxial stresses to failure in the uniaxial stress configuration. Therefore the next step is to develop the relation between the value f_1 at failure and the uniaxial failure f_b force in the polymer chain as given by equation (1.2.4). The relationship is not one to one since a certain geometric factor has to be taken into account. Why this geometric effect should be present can easily be argued as follows. A polymer chain oriented in the direction of the load in the uniaxial case has under a given load a certain length which is related to the extension of the specimen. If now the

transverse tensile stresses are applied to the specimen, the extension of the specimen in the direction of the original load will decrease. Therefore this implies that the polymer chains carrying the original load will also contract and therefore, the effective angle that it will make with the direction of the original load will decrease. Similar argument holds if the transverse load is compressive, however now there will be an additional extension and not contraction of the polymer chains. Now since the total load in the original direction is the same, it follows that the tension in each chain must increase so that the resultant component must be equal to the original load. This effect will now be put in a mathematical form.

Consider a typical polymer chain which carries a portion of the load in a uniaxial specimen. It is assumed that on the average this chain is inclined at angle θ_u to the direction of the load. This situation is illustrated in Figure 1.11. If the effective amount of the applied load that this chain carries is denoted by f_u then the actual tension T in the chain is given by

$$T = \frac{f_u}{\cos \theta_u} \tag{1.2.20}$$

Now consider the material under multiaxial stressing. The same polymer chain will now be subject to some additional lateral forces as shown in Figure 1.11. Thus the chain will be inclined on the average at an angle θ_1 to the original uniaxial loading direction and therefore, if the actual tension in the chain at break is assumed to be the same as in the uniaxial case, the effective load that the chain can carry is now

$$f_1 = T \cos \theta_1 \tag{1.2.21}$$

and using equation (1.2.20) and eliminating T we get

$$f_1 = \frac{\cos \theta_1}{\cos \theta_u} f_u \tag{1.2.22}$$

Therefore for a given same relaxation state the ratio of the effective loads that a uniaxial and a multiaxial specimen can carry is given by

$$\frac{\sigma_u}{\sigma_1} = \frac{f_u}{f_1} = \frac{\cos \theta_u}{\cos \theta_1} \tag{1.2.23}$$

As pointed out above the comparison must be made at some equal "state of relaxation" and therefore we choose to use as the standard the long time (rubbery) state, which, for the multiaxial case, was defined above. We shall now relate the ratio in equation (1.2.23) to the relative extensions. Consider, see Figure 1.11, that the polymer chain has some cross-sectional area a associated with it. Therefore in the case of the uniaxial loading the effective area of the chain, perpendicular to the load, will be $a/\cos\theta_u$. Similarly for the case of a multiaxial situation the same effective cross-section will be $a/\cos\theta_1$. However the ratio state of the cross-sections at the rubbery state, is $\lambda_{t_R} / \lambda_{2_R} \lambda_{3_R}$; where λ_{t_R} is rubbery uniaxial transverse extension and λ_{2_R} and λ_{3_R} are the relative extensions for multiaxial case corresponding to a rubbery response in the direction 1. Therefore we have

$$\frac{\cos\theta_1}{\cos\theta_u} = \frac{\lambda^2_{t_R}}{\lambda_{2_R}\lambda_{3_R}} \tag{1.2.24}$$

and from equations (1.2.23) and (1.2.24) we have

$$f_1 = f_u \frac{\lambda^2_{t_R}}{\lambda_{2_R}\lambda_{3_R}} \tag{1.2.25}$$

Combining equations (1.2.13), (1.2.19) and (1.2.25) we obtain

$$f_1 = f_u \frac{\lambda^2_{t_R}}{\lambda_{2_R}\lambda_{3_R}} = \frac{\sigma_1}{g} \tag{1.2.26}$$

or

$$f_u = \frac{\sigma_1 \lambda_{2_R}\lambda_{3_R}}{\lambda^2_{t_R}} \tag{1.2.27}$$

The failure will occur in the direction 1 if the right hand side of equation (1.2.27) approaches the value f_b, which is the critical value obtained from the uniaxial case. Since from the uniaxial failure data the product $f_b g$ is known, we rewrite equation (1.2.27) as follows

$$f_u g = \frac{\sigma_1 \lambda_{2_R} \lambda_{3_R}}{\lambda^2_{t_R}} \qquad (1.2.28)$$

and the failure criterion can be restated as follows: failure will occur in the direction of the axis 1 in Figure 1.10 when the right hand side of equation (1.2.28) becomes equal to the product $f_b g$, where the latter is the failure condition obtained from the uniaxial data. When the right hand side of equation (1.2.28) is less than the product $f_b g$, then there will be no failure. Since it is necessary to investigate failure conditions along all directions in the material it is necessary to apply the above analysis to all possible orientations of the coordinate system shown in Figure 1.10. When along one direction the failure criterion will be satisfied then the failure of the whole material will be said to have occurred.

It is interesting at this point to note that in the limit of long time response, equation (1.2.28) provides a failure criterion for multiaxial situations under slow rates of testing. Therefore, it would be possible to check the geometric effects in the present theory by comparing the present criterion with experimental data from slow, rubbery, rates of test. Such a check could perhaps reveal any possible improvements in the form of the geometric corrections represented by equation (1.2.25).

The final verification of the present failure theory can only be obtained by experiments. To explore the ramifications proposed herein, an extensive testing program has been initiated at GALCIT to conduct failure tests on uniaxial, biaxial and triaxial specimens subjected to variable strain rates and temperatures. It is hoped that these tests will provide data which can be used to check critically the present theory for the three particular situations mentioned. These tests and the results will be discussed in subsequent sections of this report.

REFERENCES

1.1 Lindsey, G. H.; Schapery, R. A.; Williams, M. L.; Zak, A. R.: "The Triaxial Tension Failure of Viscoelastic Materials," ARL 63-152, Aeronautical Research Laboratories, United States Air Force, Dayton, Ohio, September 1963.

1.2 Rivlin, R. S.; Thomas, A. G.: "Rupture of Rubber, I. Characteristic Energy of Tearing," Journal of Polymer Science, Vol. 10, No. 3, p. 291, 1953.

1.3 Thomas, A. G.: "Rupture of Rubber, II. The Strain Concentration at an Incision." Journal of Polymer Science, Vol. 18, p. 177, 1955.

1.4 Greensmith, H. W.; Thomas, A. G.: "Rupture of Rubber, III. Determination of Tear Properties," Journal of Polymer Science, Vol. 18, p. 189, 1955.

1.5 Greensmith, H. W.: "Rupture of Rubber, IV. Tear Properties of Vulcanizates Containing Carbon Black," Journal of Polymer Science, Vol. 21, p. 175, 1956.

1.6 Thomas, A. G.: "Rupture of Rubber, VI. Further Experiments on the Tear Criteria," Journal of Applied Polymer Science, Vol. 3, No. 8, p. 168, 1960.

1.7 Schapery, R. A.; Williams, M. L.: "On the Acceleration of Cracks in Viscoelastic Media," GALCIT SM 62-39, California Institute of Technology, September 1962.

1.8 Knauss, W. G.: "Rupture Phenomena in Viscoelastic Materials." Ph. D. Dissertation in Aeronautics, California Institute of Technology, GALCIT SM 63-10, June 1963.

1.9 Williams, M. L.: "The Structural Analysis of Viscoelastic Materials," GALCIT SM 63-15, California Institute of Technology. May 1963. AIAA Journal, Vol. 2, No. 5, May 1964, pp. 785 - 809.

1.10 Smith, T. L.: "Dependence of the Ultimate Properties of GR-S Rubber on Strain Rate and Temperature," Journal of Polymer Science, Vol. 32, p. 99, 1958.

1.11 Williams, M. L.; Landel, R. F.: and Ferry, J. D.: "The Temperature Dependence of Relaxation Mechanisms in Amorphous Polymers and Other Glass-Forming Liquids," Journal of American Chemical Society, Vol. 77, p. 3701, 1955.

1.12 Bueche, F.; Halpin, J. C.: "Molecular Theory for the Tensile Strength of Gum Rubbers," The Goodyear Tire and Rubber Company Dept., No. 5, from Physics Department, University of Dayton, April 1963.

1.13 Smith, T. L.; Stedry, P. J.: "Time and Temperature Dependence of the Ultimate Properties of an SBR Rubber at Constant Elongations," Journal of Applied Physics, Vol. 31, p. 1892, 1960.

1.14 Smith, T. L.: "Ultimate Tensile Properties of Rubberlike High Polymers," Proceedings Division of Organic Castings and Plastics Chemistry, Chicago Meeting of the American Chemical Society, September 1961, p. 168.

1.15 Landel, R. F.: "The Tensile Behavior of Composite Propellants," SPIA, 20th Meeting Bulletin, JANAFAN Panel on Physical Properties of Solid Propellants, Vol. 1, p. 357, 1961.

1.16 Gent, A. N.; Lindley, P. B.: "Internal Rupture of Bonded Rubber Cylinders in Tension," Proceedings of the Royal Society A, Vol. 249, p. 195, 1959.

1.17 Blatz, P. J.; Ko, W. L.; Zak, A. R.: "Fundamental Studies Relating to the Mechanical Behavior of Solid Propellants, Rocket Grains and Rocket Motors," California Institute of Technology, GALCIT SM 61-15, 61-19, 62-14, 62-23, 62-27, 63-5, 63-17, and 63-33.

1.18 Tobolsky, A.; Eyring, H.: "Mechanical Properties of Polymer Materials," Journal of American Physics, Vol. 2, p. 125, March 1943.

1.19 Taylor, G. R.; Darin, S. R.: "The Tensile Strength of Elastomers," Journal of Polymer Science, Vol. 17, p. 511, 1955.

1.20 Bueche, . . M.: "Ultimate Properties of Simple Elastomers," Journal of Polymer Science, Vol. 19, p. 275, 1956.

1.21 Bueche, F.: "Tensile Strength of Rubbers," Journal of Polymer Science, Vol. 24, p. 189, 1957.

1.22 Bueche, F.: "Tensile Strength of Plastics Above the Glass Temperature," Journal of Applied Physics, Vol. 26, No. 9, p. 1133, September 1955.

1.23 Bueche, F.: "Tensile Strength of Plastics, Effect of Flows and Chain Relaxation," Journal of Applied Physics, Vol. 29, No. 8, p. 1231, August 1958.

1.24 Bueche, F.: "Physical Properties of Polymers," Interscience Publishers, p. 262, 1962.

1.25 Guth, E.; Wack, P. E.; Anthony, R. L.: "Significance of the Equation of State for Rubber," Journal of Applied Physics, Vol. 17, p. 347, 1946.

1.26 Leaderman, H.: "Large Longitudinal Retarded Deformations of Rubberlike Network Polymers," Transactions of the Society of Rheology, Vol. 6, p. 361, 1962.

1.27 Smith, T. L.: "Stress-Strain-Time Temperature Relationship for Polymers," Reprint from Symposium on Stress-Strain-Time Temperature Relationships in Materials, Special Technical Publication No. 325, ASME.

1.28 Martin, G. M.; Roth, F. L.; Stiehler, R. D.: "Behavior of Pure-Gum Rubber Vulcanizates in Tension," Transactions, Institute of Rubber Industry, Vol. 32, p. 189, 1956.

1.29 Britton, S. C.; Corley, B. M.; and Hall, R. L.: "Triaxial Tensile Stress Evaluation of Propellant-to-Case Bond Integrity," Presented at the AIAA Solid Propellant Rocket Conference, Palo Alto, California January 1964, Paper No. 64-152.

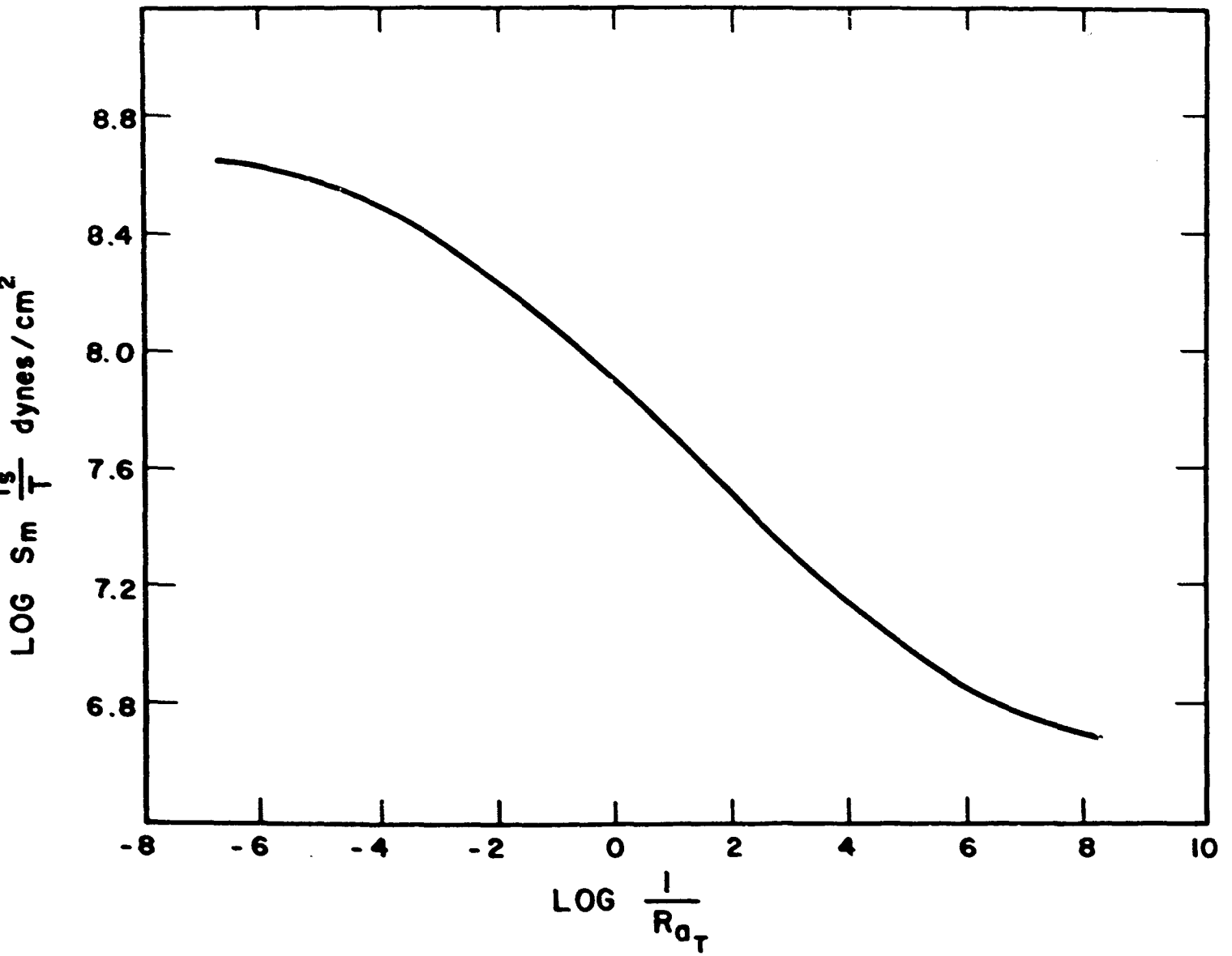

Fig. 1.1. Ultimate Tensile Strength of SBR Gum Vulcanizate at Different Strain Rates Reduced to One Temperature.

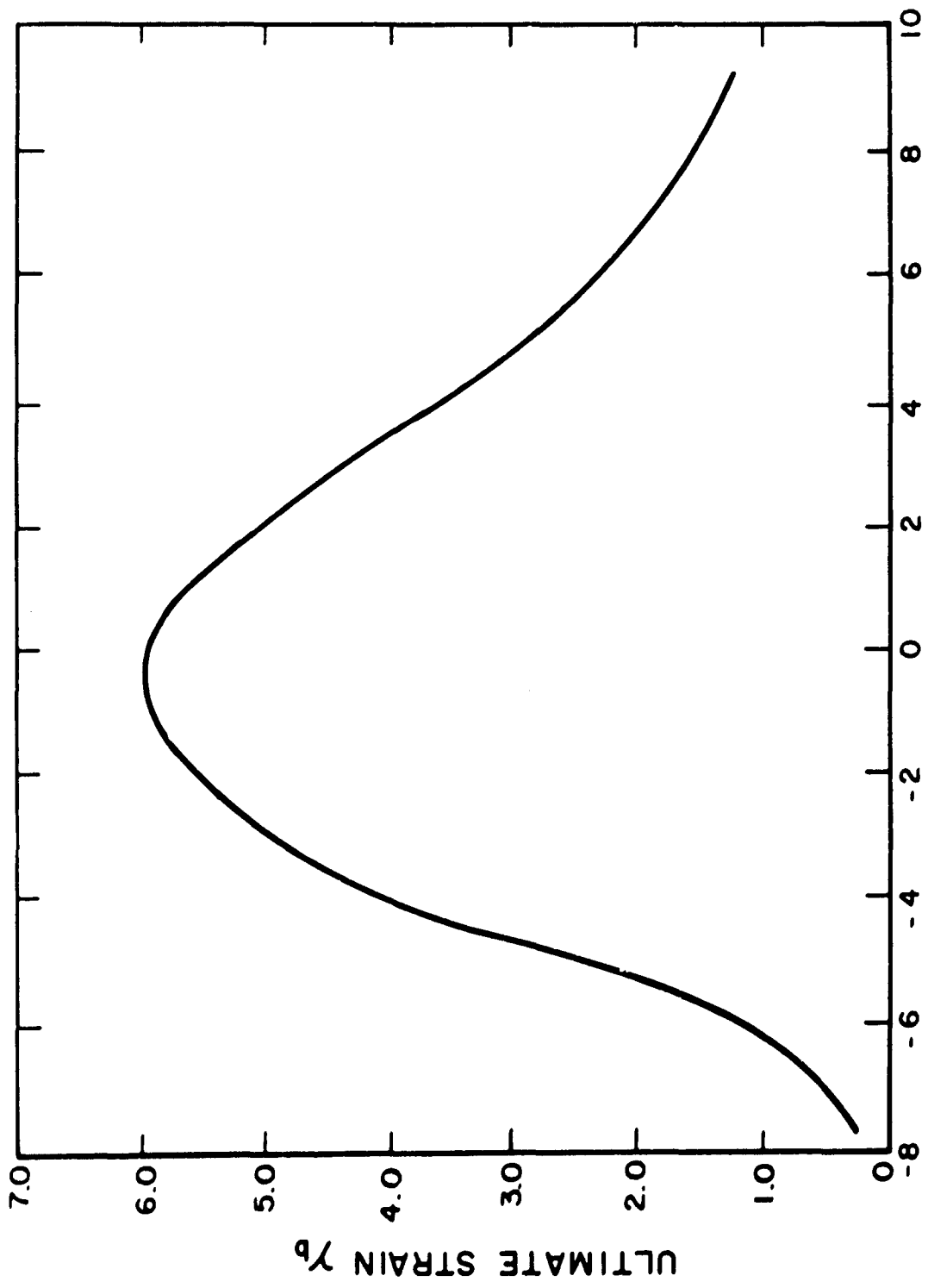

Fig. 1.2. Ultimate Strain of SBR Gum Vulcanizate at Different Strain Rates Reduced to One Temperature.

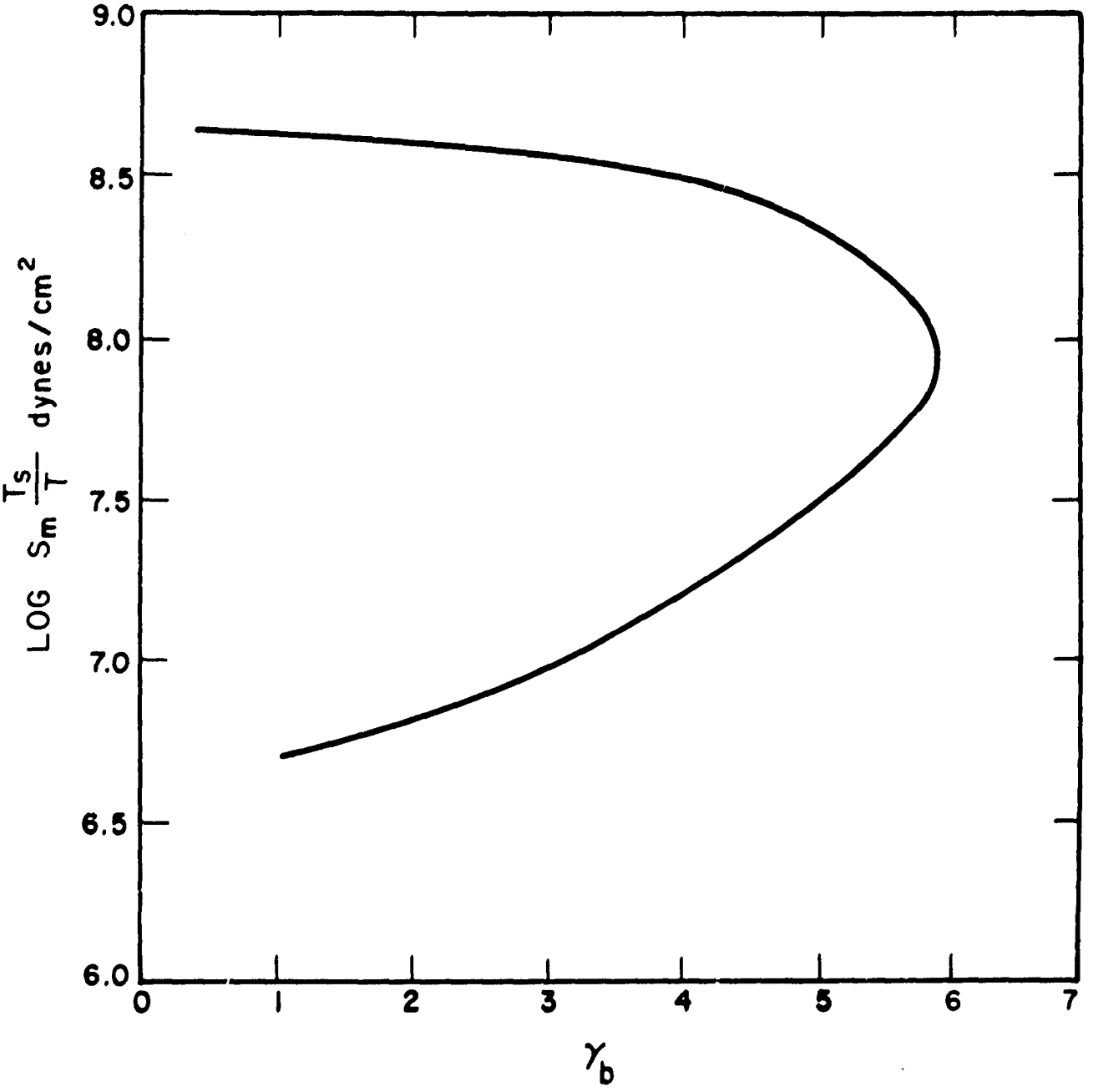

Fig. 1.3. Failure Envelope of SBR Gum Vulcanisate.

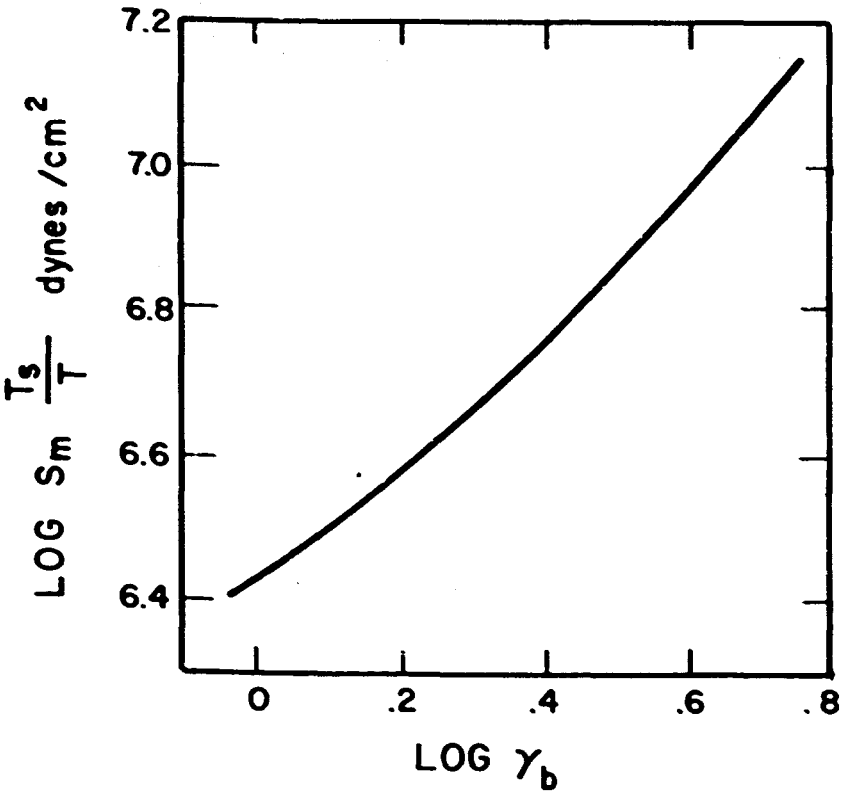

Fig. 1.4. Failure Envelope of SBR Gum Vulcanizate Given by Ultimate Property Values Observed Under Constant Strain Conditions.

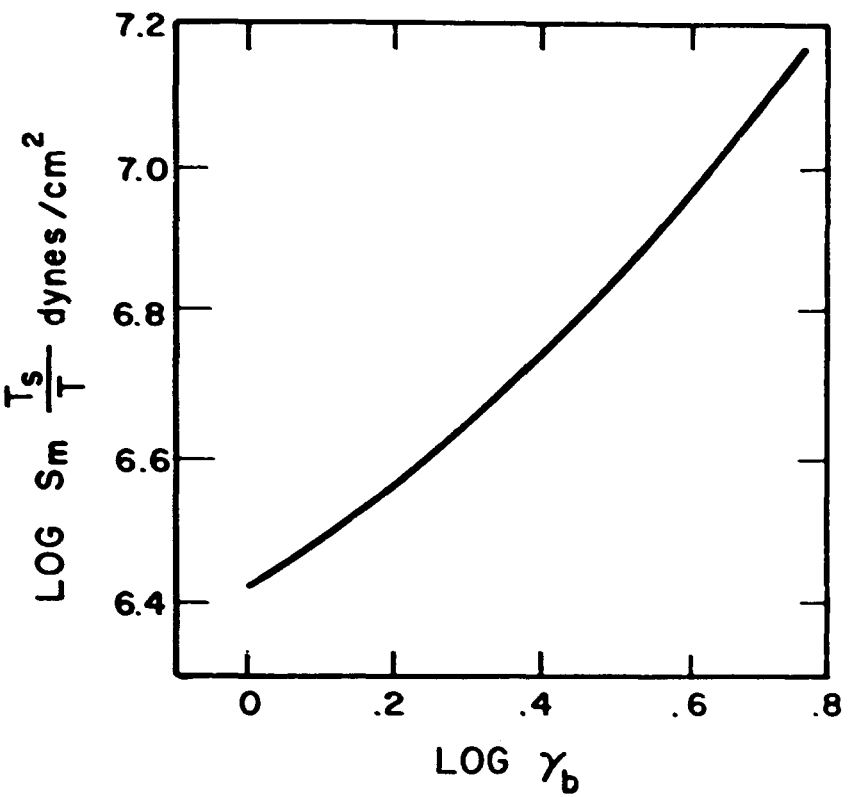

Fig. 1.5. Failure Envelope for SBR Gum Vulcanizate given by Ultimate Property Values Observed Under Costant Strain Rate Conditions.

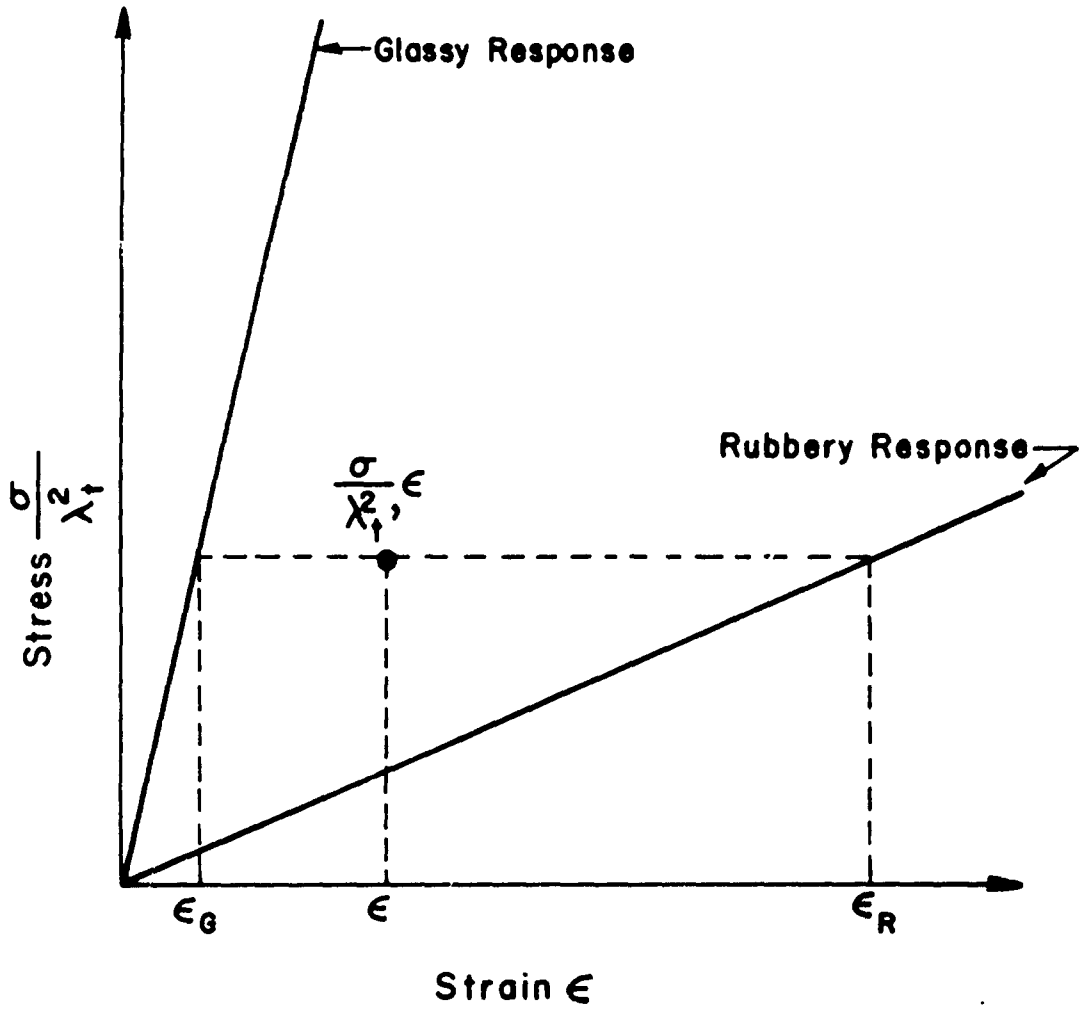

Fig. 1.6. Schematic Representation of a Stress-Strain Plane for a Viscoelastic Material.

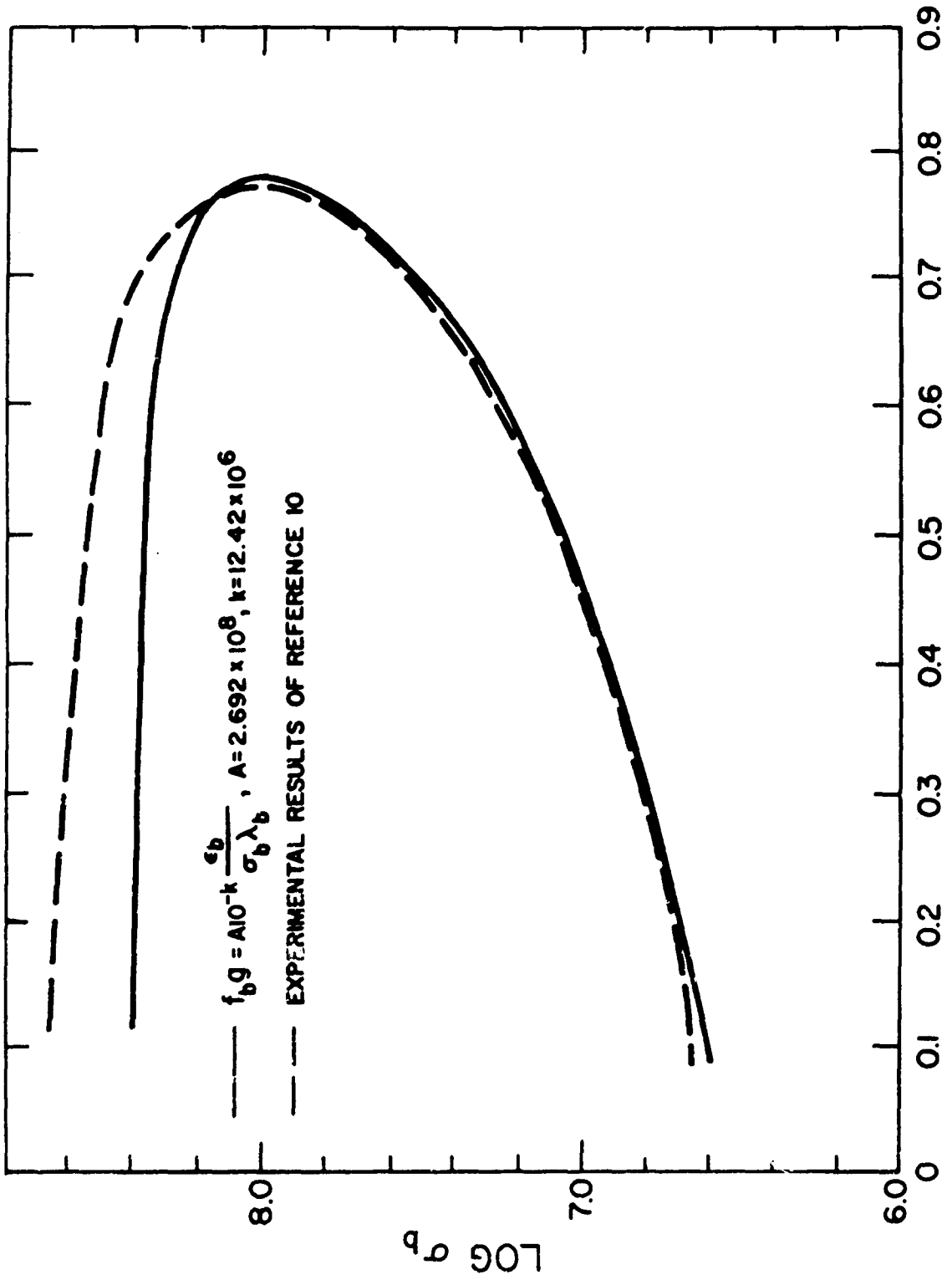

Fig. 1.7. Comparison of the Failure Envelope Obtained from the Present Theory with the Experimental Results on SBR.

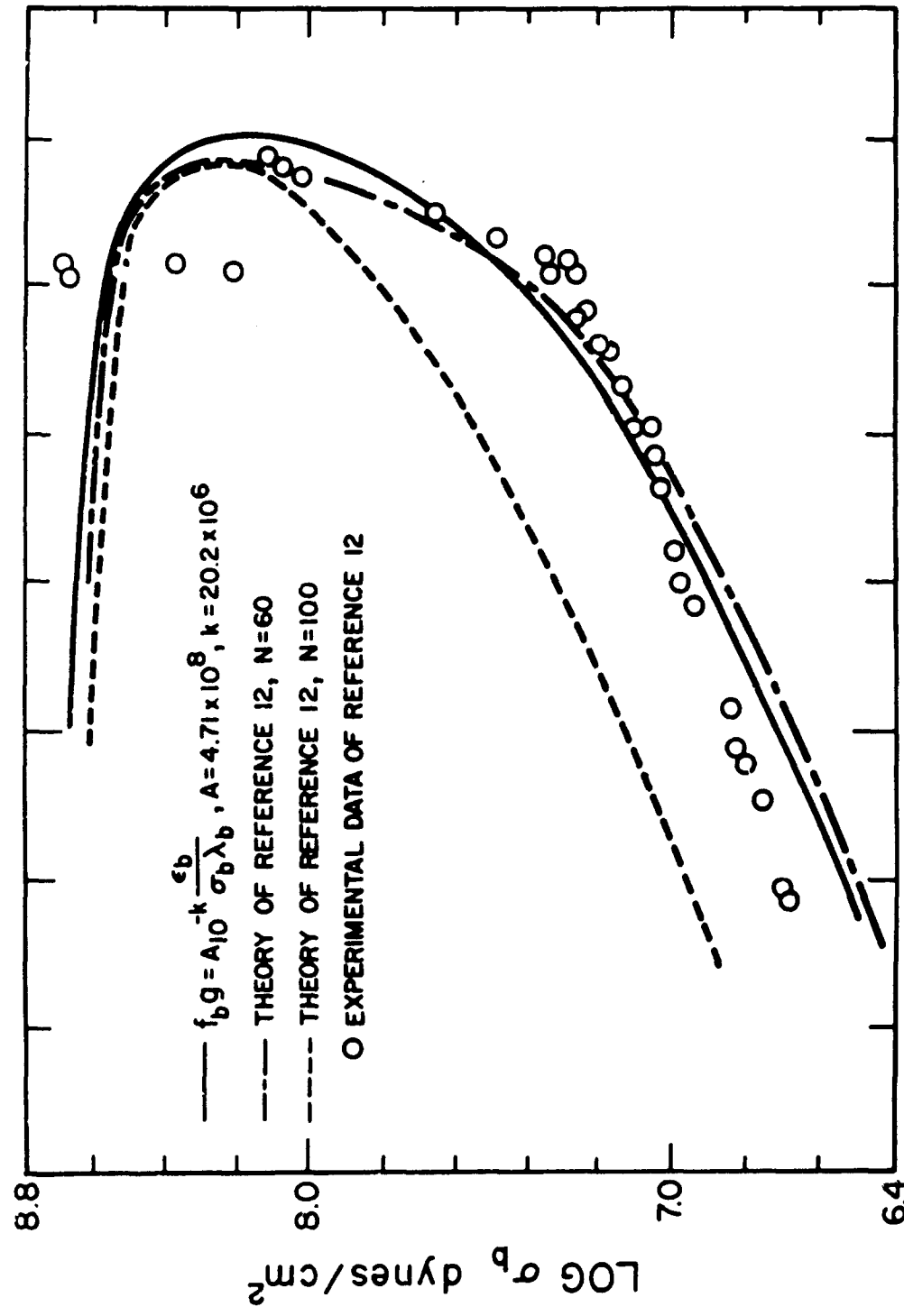

Fig. 1.8. Comparison of the Failure Envelope Obtained from the Present Theory with the Experimental Results and the Theory of Reference 1.12 for SBR Vulcanizate.

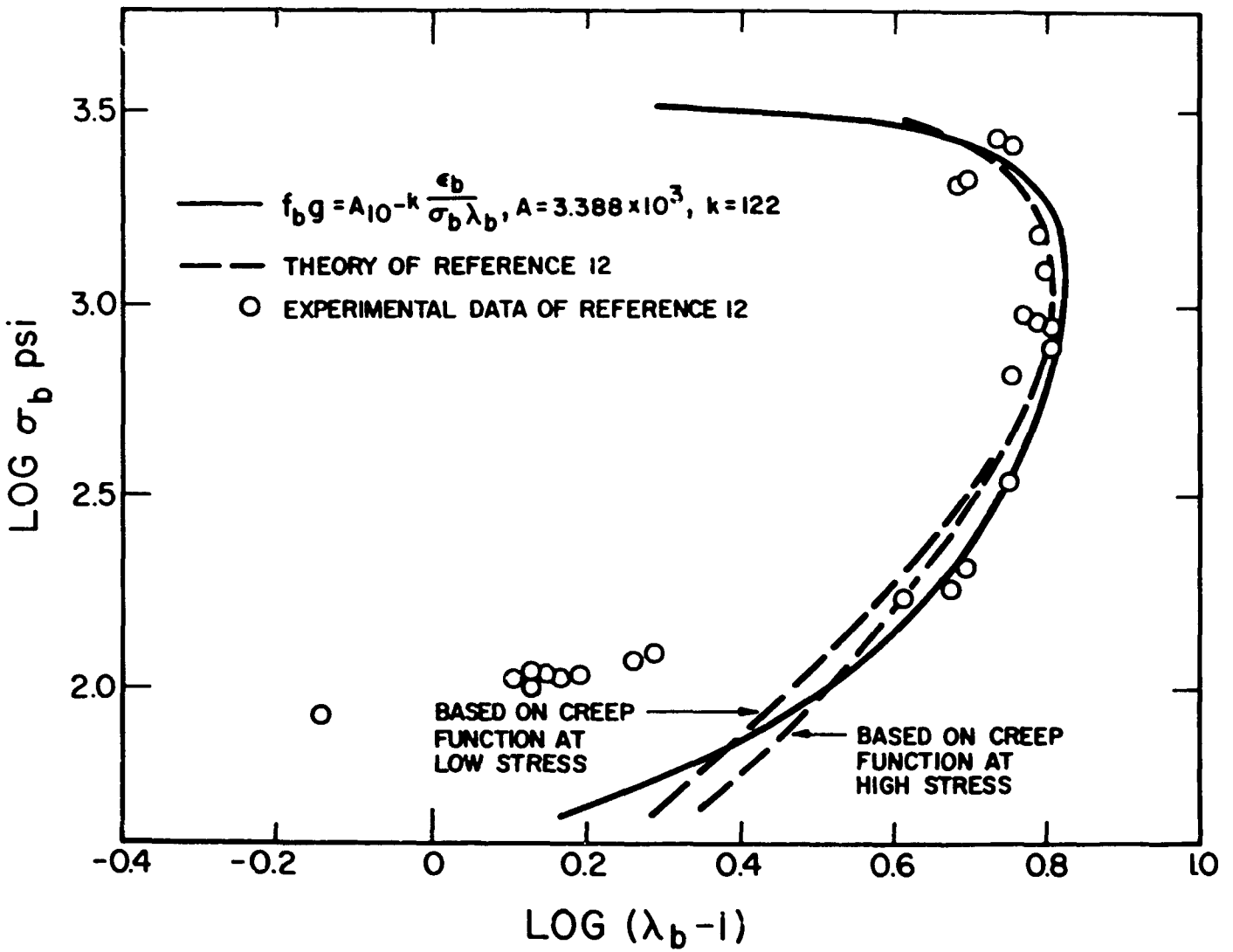

Fig. 1.9. Comparison of the Failure Envelope obtained from the Present Theory with the Experimental Results and the Theory of Reference 1.12 for Ethylene Propylene Vulcanizate.

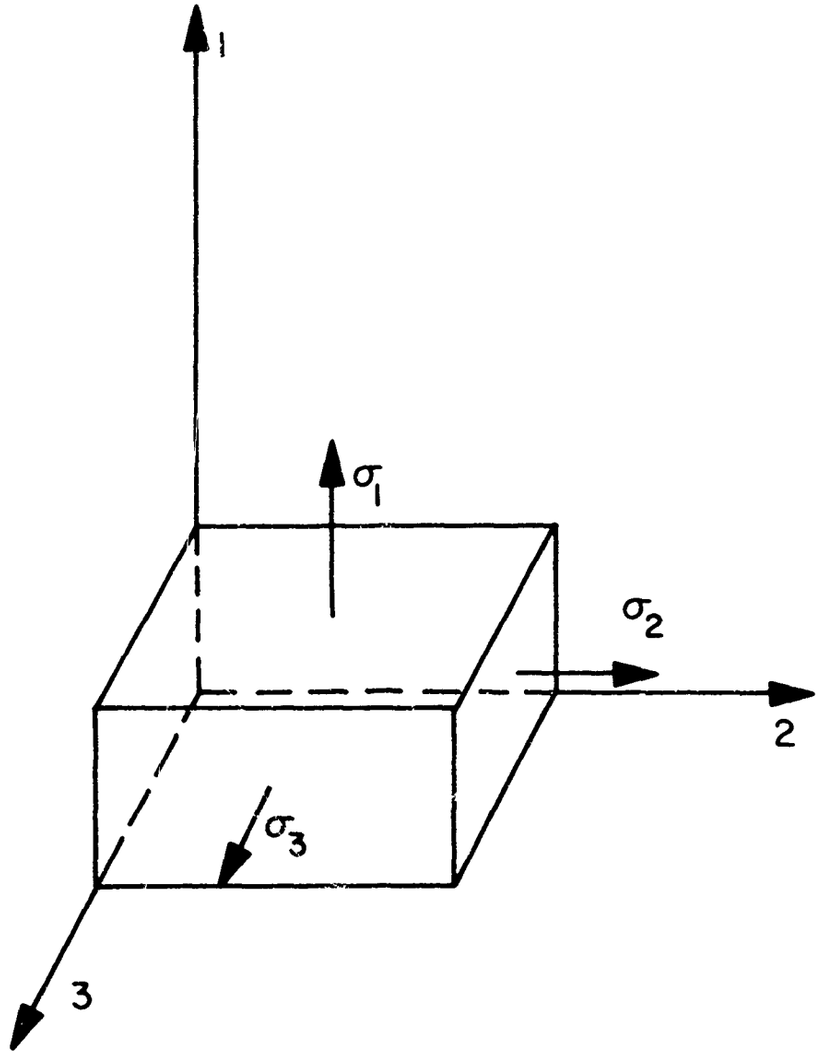

Fig. 1.10. Multiaxial Stress State Referred to a Cartesian Orthogonal Coordinate System.

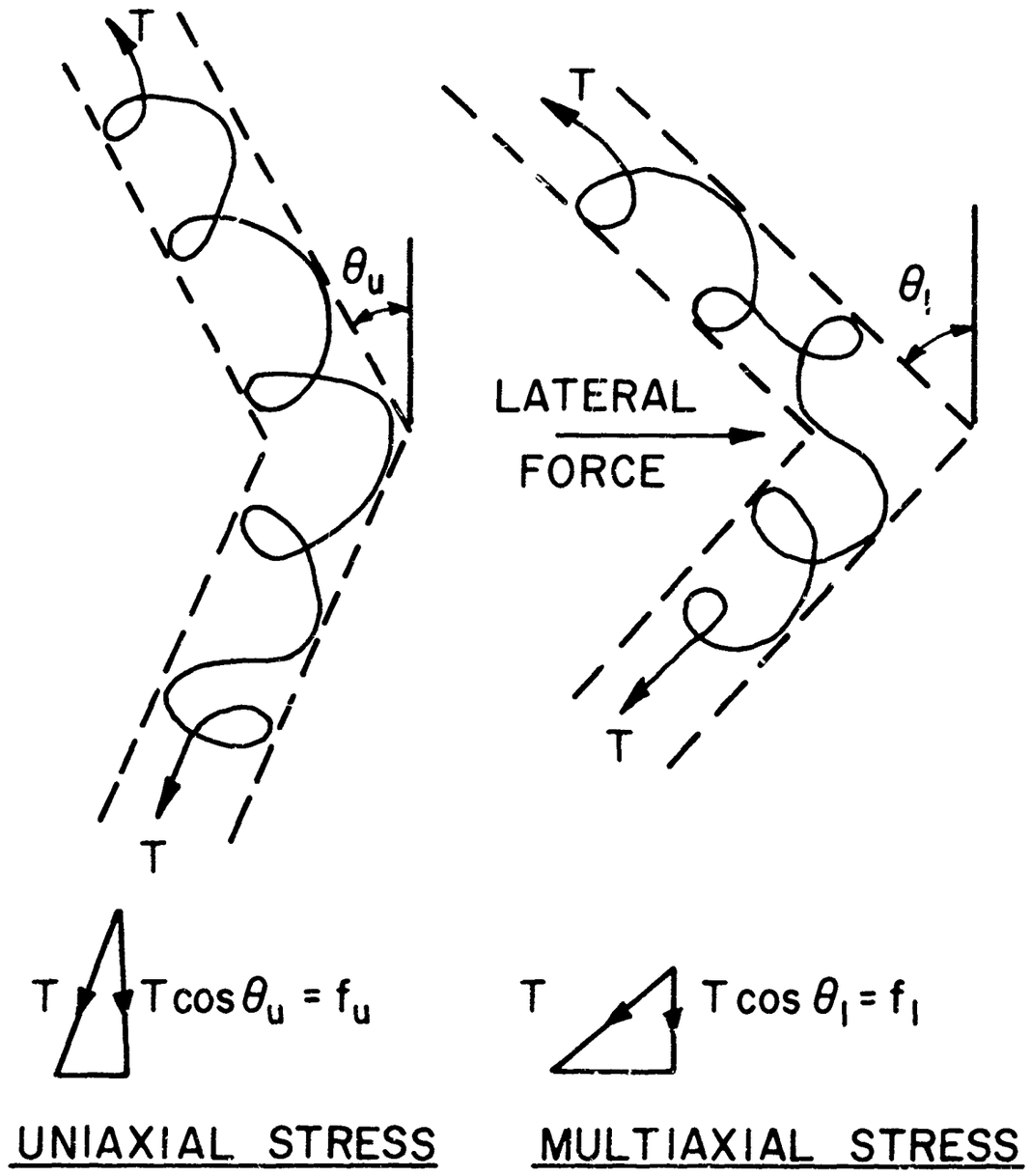

Fig. 1.11. Schematic Representation of a Polymer Chain Subject to Uniaxial and Multiaxial Stress Conditions.

2.0 VISCOELASTIC ANALYSIS OF THE POKER-CHIP TRIAXIAL STRESS SPECIMEN

2.1 INTRODUCTION

As indicated in the previous section of this report, "poker-chip" triaxial tests are being conducted in order to obtain failure data under multiaxial stress conditions. The first set of these tests has now been completed and the results will be discussed later in this report. The tests have been carried out under various strain rates and temperatures in order to evaluate the viscoelastic effects on multiaxial fracture and provide data to compare with the failure theory which was developed in the previous section. In order to intepret this data it is necessary that the stresses and strains may be known under any conditions of strain rate and temperature. This in turn necessitates that a viscoelastic stress analysis of the "poker-chip" specimen be carried out. In the present section we shall describe such analysis.

In Section 3.0 of the previous Interim Report[2.1]* the elastic analysis of the "poker-chip" specimen was developed and presented. We shall use this analysis in the present section as a basis to develop the viscoelastic stress situation. Alfrey[2.2] was the first to propose an analogy between certain elastic and linear viscoelastic problems. The analogy depends on the fact that governing equations in a viscoelastic medium can be transformed by application of Laplace Transforms. The resulting equation and the corresponding boundary conditions have the same form as an associated elastic problem. The elastic constants in this associated elastic problem become the transformed viscoelastic material properties. This approach was subsequently extended by Tsien[2.3] and Lee[2.4] and described for engineering analysis by Williams[2.5]. This method will be used here to obtain the viscoelastic solution for the stress and strains in the "poker-chip" subject to time dependent strain.

2.2 VISCOELASTIC ANALYSIS

In Section 3.2.2 of reference 2.1 the elastic stresses are given for the "poker-chip" specimen, these expressions were obtained from the elastic solutions of that section

---

* Superscripts refer to references at the end of the section.

$$\frac{\sigma_r}{E\epsilon} = \left(\frac{3\nu}{1+\nu}\right)\frac{k}{E}\left[1 - \frac{I_0(r\sqrt{M})\left\{1-\frac{2}{3}M\frac{I_1(r\sqrt{M})}{r\sqrt{M}\,I_0(r\sqrt{M})}\right\}}{I_0(a\sqrt{M})\left\{1-\frac{2}{3}M\frac{I_1(a\sqrt{M})}{a\sqrt{M}\,I_0(a\sqrt{M})}\right\}}\right] \qquad (2.2.1)$$

$$\frac{\sigma_\theta}{E\epsilon} = \frac{\sigma_r}{E\epsilon} + \frac{1}{1+\nu}\left[\frac{I_0(r\sqrt{M}) - \frac{2I_1(r\sqrt{M})}{r\sqrt{M}}}{I_0(a\sqrt{M}) + \left(\frac{1-2\nu}{\nu}\right)\left\{I_0(a\sqrt{M}) - \frac{I_1(a\sqrt{M})}{a\sqrt{M}}\right\}}\right] \qquad (2.2.2)$$

$$\frac{\sigma_z}{E\epsilon} = \frac{\sigma_r}{E\epsilon} + \frac{1}{1+\nu}\left[1 + \frac{I_0(r\sqrt{M}) - \frac{I_1(r\sqrt{M})}{r\sqrt{M}}}{I_0(a\sqrt{M}) + \left(\frac{1-2\nu}{\nu}\right)\left\{I_0(a\sqrt{M}) - \frac{I_1(a\sqrt{M})}{a\sqrt{M}}\right\}}\right] \qquad (2.2.3)$$

$$\frac{\tau_{rz}}{E\epsilon} = \left(\frac{3\nu}{1+\nu}\right)\frac{k}{E}\,\frac{\sqrt{M}}{\left[1-\frac{2}{3}M\left(\frac{I_1(a\sqrt{M})}{a\sqrt{M}\,I_0(a\sqrt{M})}\right)\right]}\left[\frac{I_1(r\sqrt{M})}{I_0(a\sqrt{M})}\right]Z \qquad (2.2.4)$$

Also according to this solution the radial and the axial displacements are

$$u = -(1-z^2)\, g\,(r) \tag{2.2.5}$$

$$w = \epsilon z \tag{2.2.6}$$

where

$$g(r) = A\, I_1\left(r\sqrt{M}\right) \tag{2.2.7}$$

and

$$A = \frac{3}{2}\,\frac{\nu\epsilon}{(1-\nu)\sqrt{M}\; I_0\left(a\sqrt{M}\right) - (1-2\nu)\,\dfrac{I_1\left(a\sqrt{M}\right)}{a}} \tag{2.2.8}$$

where

$$M = \frac{3}{2}\,\frac{(1-2\nu)}{(1-\nu)} \tag{2.2.9}$$

The cylindrical coordinates to which this solution is referred are illustrated in Figure 2.1. The above equations (2.2.1) to (2.2.9) are sufficient to describe the elastic stress and the strain state at any point in the specimen.

Using the Alfrey analogy the solution for the associated elastic problem corresponding to the viscoelastic situation can immediately be obtained in the transformed plane. As indicated in reference 2.5 this is done by simply replacing the stress and the displacements by their Laplace transforms and replacing the three physical constants E, K, and ν by their counterparts. The strain input $\epsilon(t)$ to the specimen is replaced by the transform of the time dependent input $\bar{\epsilon}(p)$, where p is the Laplace transform variable. If the inverse transform can be carried out of the resulting equations, the viscoelastic solution of the "poker-chip" specimen will be complete. However, only a brief examination of the functions involved in these expressions will show that their complex nature precludes the possibility of a practical exact inverse. Therefore, the use of approximate methods becomes necessary.

Two such approximate methods have been developed by Schapery[2.6]; one is referred to as the direct method and the other as the collocation method. In the direct method, which is valid for quantities varying slowly with respect to time on the logarithmic scale, the Laplace transform variable is replaced by the factor 0.5/t where t is the time, to obtain the approximate solution. In the collocation approach the physical unknown quantities are assumed in Dirichlet series form, for example

$$S = S_o + \sum_{i=1}^{n} S_i \, e^{-\frac{t}{\tau_i}} \qquad (2.2.10)$$

The quantities τ_i are assumed to cover the time range of the expected response of the solution and the coefficients S_i are evaluated by minimizing the square of the error in the transformed plane.

We shall consider both of these approximations for the final solution of the viscoelastic "poker-chip" problem. However, before such a solution is carried out to completion it is necessary that the viscoelastic material properties be known. At the present time the Solithane 113 material, which is being used for the poker-chip tests, has not been completely characterized for the viscoelastic properties. And, therefore, the analysis of the present section cannot be completed at this time and this will be done as the characterization data becomes available. The characterization tests are now being conducted in conjunction with the failure tests mentioned previously and this experimental program will be discussed in the latter section of this report.

REFERENCES

2.1 Lindsey, et al,: "The Triaxial Tension Failure of Viscoelastic Materials," ARL 63-152, Aerospace Research Laboratories, United States Air Force, September 1963.

2.2 Alfrey, T.: "Non-Homogeneous Stresses in Viscoelastic Media," Quarterly of Applied Mechanics, Vol. 2, p. 113, 1944.

2.3 Tsien, H. S.: "A Generalization of Alfrey's Theorem for Viscoelastic Media," Quarterly of Applied Mathematics, Vol. 8, p. 104, 1950.

2.4 Lee, E. H.: "Stress Analysis in Viscoelastic Bodies," Brown University, Division of Applied Mathematics, Technical Report No. 8.

2.5 Williams, M. L.: "The Structural Analysis of Viscoelastic Materials," GALCIT SM 63-15, California Institute of Technology, May 1963. AIAA Journal, Vol. 2, No. 5, May 1964, pp. 785-809.

2.6 Schapery, R. A.: "Approximate Methods of Transform Inversion for Viscoelastic Stress Analysis," Proceedings of the Fourth U. S. Congress of Applied Mechanics, Berkeley, California, June 1962.

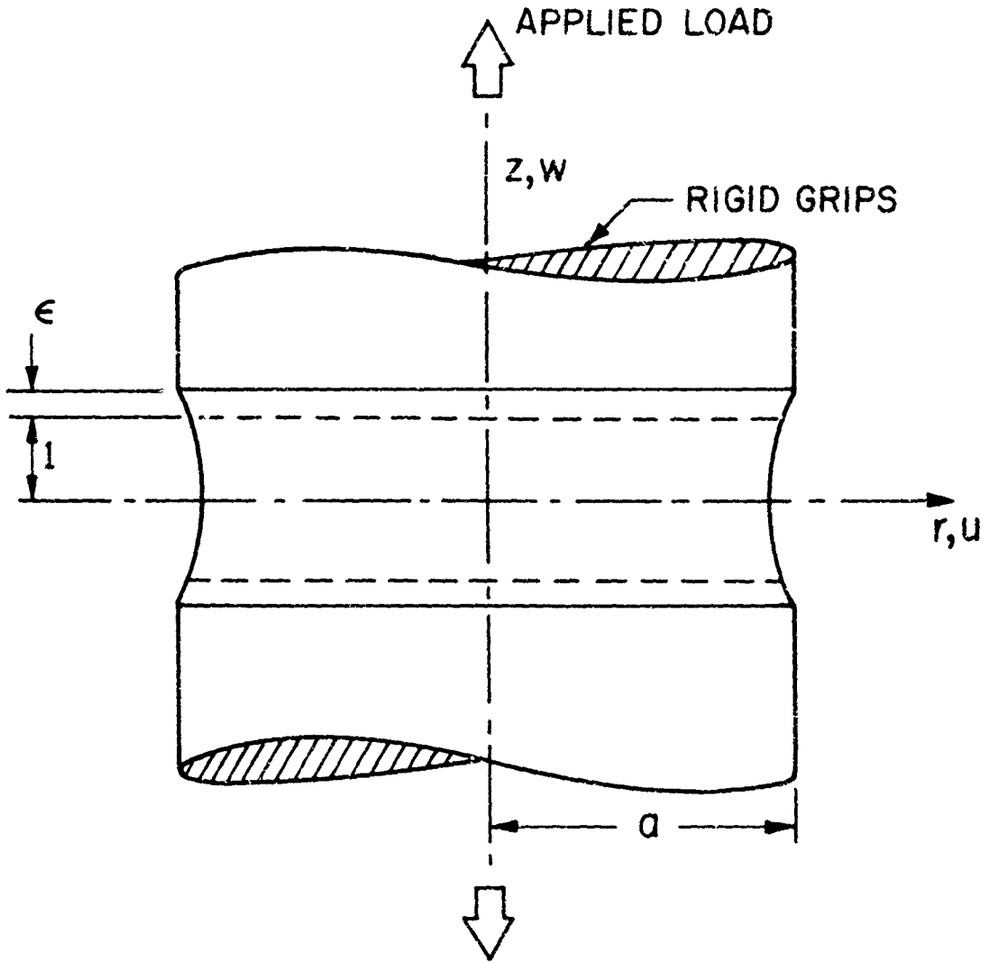

Fig. 2.1. Triaxial "Poker-Chip" Test and the Coordinate System Used in the Stress Analysis.

3.0 POLYMER MATERIAL MANUFACTURING FACILITY

3.1 INTRODUCTION

After considering its various advantages, Solithane 113 polyurethane polymeric material was chosen for the experimental portion of this investigation. Apart from the viscoelastic mechanical properties Solithane 113 possesses well pronounced birefringent properties and is a very clear material. The latter two properties make this material very suitable for photoviscoelastic studies. Another factor which entered into the choice of this material was the fact that it was already being made by the Jet Propulsion Laboratories of the California Institute of Technology and these facilities were made available for use in the early stages of this project. After a certain amount of experimental data was obtained and disseminated it became obvious that the mechanical properties of the material possessed a sizable variation from one sample to another. At that stage it became obvious that the reason for this could lay in the manufacturing process because the manner in which this material was made did not provide sufficiently close control of conditions at all stages of the process. It was therefore decided to build a casting facility at GALCIT which would overcome these difficulties. The facility uses a completely different process which is designed so that maximum control can be achieved at all stages of the manufacturing cycle.

In the area of mechanical testing of polymeric materials there has existed for a long time a need for standardized materials. If such a material or materials could be developed and accepted, the various research organizations could work with the same material and accumulate characterization data on cooperative basis. Such a program would forseeably lead to well characterized materials which would be most suitable for further basic material research and analytical studies. The manufacturing process for any such standard material will have to be well established so that various organizations can reproduce exactly the same material. Some researchers interested in this standard materials program have expressed the opinion that the Solithane 113 could perhaps be suitable for this purpose. It is appropriate therefore, that the present manufacturing process, developed and perfected at GALCIT, could be considered for use by other organizations. Therefore the manufacturing facility and process will now be described in detail.

3.2 GENERAL DESCRIPTION OF THE MANUFACTURING FACILITY

The Solithane 113 manufacturing facility is shown in the photographs of Figures 3.1 to 3.6. The facility is physically divided into two parts, the preheating and mixing machine, and the mold and curing oven. The overall view of the pre-heating and the mixing machine is shown in Figure 3.1. The two components which go into the making of the Solithane 113 are preheated in specially constructed two gallon tanks which can be partially seen in Figure 3.2. These tanks were made from standard spray-paint containers which have been modified for the purpose. The tank which holds the prepolymer and the tank for the catalyst are identical in construction. The following description applies to both. The tank is filled and emptied through a long copper tube shown on the schematic diagram, Figure 3.7; this tube reaches nearly to the bottom of the tank. Another tube, used for evacuating or pressurizing the tank, enters the tank also through the top and ends near the top. The contents of the tank are agitated by a mechanical stirrer which is also shown in Figure 3.7. This stirrer is driven by a pulley and belt arrangement which can be seen in Figure 3.4. Except for the main seal between the tank and its top, which is of rubber, all the other seals and bushings are of teflon. The shaft of the stirrer is sealed with a teflon O-ring. The temperature of the tank contents is measured with a copper constantan thermocouple which is inside a brass tube which in turn projects down from the top of the tank. The output of the thermocouple is read on a Leeds and Northrup potentiometer. The valve system for each tank is shown schematically in Figure 3.7. The function of each valve will be described later.

The two tanks just described sit inside a bigger tank which can be seen in Figure 3.2. During the operation, water is circulated in this tank in order to preheat the contents of the two smaller tanks. The water is agitated mechanically by the stirrer which can be seen in Figure 3.2. This tank possesses a double wall with insulation in between. With this arrangement the temperature of the total system can be kept constant for long times. The temperature of the water in this tank is read with a thermocouple and a mercury thermometer. The top of the tank is covered with an aluminum cover, seen in Figure 3.4. This cover supports the pulley and belt system for the three stirrers and the valve assembly for the two individual internal tanks. The power for the stirring is provided by a variable speed motor

which can be seen in Figure 3. 3. On the top of the assembly and to the right of the water tank there are additional valves necessary for the vacuum system. The vacuum pump is situated below the water tank. The valves for the vacuum and the nitrogen system are brass and for the portions of the system through which the polymer components flow, the valves are brass with teflon seals. It was found that these valves give the best service. Attached to the front of the top of the water tank is a switching terminal which permits rapid reading of the different thermocouples in the system.

To the right of the water tank a vertical rack supports two measuring burets, one for each of the two components of the polymer, and a mixing flask in which the components are mixed. This arrangement can be seen in the photograph of Figure 3. 5. The burets for the prepolymer and the catalyst are identical in construction and therefore only one description is necessary. One buret assembly and the mixing flask are shown schematically in Figure 3. 8. The measuring of the components is made of volume by filling each buret completely to overflow. The burets are immersed in a water jacket (see Figure 3. 8) through which the water is circulated from the main preheating tank. Therefore since the temperature is constant the volume measurement is equivalent to a weight measurement. As a component, prepolymer or catalyst, enter the measuring assembly it first enters into a small antechamber which is also inside the water jacket and into which the top of the buret protrudes. From this antechamber the component enters the buret and after the buret is filled the overflow remains in the compartment and can be removed through an overflow tube. A vacuum line enters the antechamber and it is used for evacuating the buret. A small flask is placed in this vacuum line in order to prevent the liquid components from being drawn into the vacuum pump. The burets can also be pressurized with nitrogen and this is done by the same tube through which the polymer component enters. The water enters the jacket through the bottom and leaves through a tube at the top. This tube is concentric with the copper line through which the burets are filled. This arrangement prevents cooling of the components as they travel from the tanks to the burets.

The components are emptied from the burets into the mixing flask, see Figure 3. 8. The flask is sitting in a beaker of boiling water which is heated by an electric element. The polymer components are mixed in this flask by a mechanical stirrer whose shaft enters at the top of the flask and is

driven by a small electric motor. The flask can be evacuated or pressurized with nitrogen atmosphere by opening appropriate valve Another tube enters the top of the flask and ends at the bottom, this tube i ed for emptying the mixture from the flask into the curing mold.

The resulting molten polymer mixture is cast and cured in an aluminum mold located in an oven. The mold and the oven can be seen in the photograph of Figure 3.6. The mold is suspended from the oven door for easy handling. The mold is circular and it splits into two halves to reveal the molding compartment. The molding compartment is approximately 14 inches in diameter and one-tenth inch thick. The internal surfaces of the molding compartment are polished to mirror finish. The material is aluminum 6061. During the casting the two halves of the mold are bolted together and the polymer mixture enters at the top through a copper tube. After curing, the two halves are separated and the solid polymer removed. Recently another mold similar in construction has been completed which enables casting of thicker polymer specimens approximately six inches square and one-half inch thick. The curing oven is electric and has automatic preselected temperature controls which can be seen on the right of Figure 3.6. The fumes which are produced during curing are removed by a hood which fits over the oven. As a double check on the curing temperature a copper constantan thermocouple is attached directly to the mold; it is read with the potentiometer.

3.3 MANUFACTURING PROCESS

Before the mixing and the casting of the Solithane 113 can begin, it is necessary to fill the two preheating tanks, Figure 3.2, with the prepolymer and the catalyst. These two components are received in the laboratory in sealed one gallon cans which have to be emptied into the respective tanks A method for doing this has been worked out which permits the transfer of the two liquid components so that they do not come into contact with air. First the two preheating tanks are evacuated by opening valve 1, shown in Figure 3.7, and leaving the remaining valves closed. A flexible tube is now connected to the right of valve 5, this tube in turn is connected to a sharp brass tube. Another tube, also ending in a sharp point, is connected to a nitrogen source and it is driven into the top of the supply can. About one-quarter psi of nitrogen pressure is introduced into the cans. Now the first

tube, which is connected to valve 5, is driven through the top of the can and the valve 5 is opened. The vacuum in the tank and the slight nitrogen pressure in the can forces the liquid into the tank.

After the transfer is complete, valve 5 is closed and after an additional one minute valve 1 is also closed. This procedure insures that if any air had leaked into the system during the transfer it will be removed. Now valve 2 is opened and the nitrogen atmosphere is introduced into the tanks. The loading of the tanks is now complete and the mixing and casting operation can begin. At the first step of this operation the hot water supply is turned on and the water tank is filled. At the same time the mechanical stirrers both in the water tank and in the two internal tanks are started. After five minutes the water pump is turned on and this circulates the water in the jackets around the burets. The vacuum pump is now started and with all the valves closed, except valves 6 and 11 in Figure 3.8, the burets and mixing flask are evacuated. The nitrogen pressure is regulated to 12 psi and valve 2 is left open. During the time that the components are approaching a thermal equilibrium the mold is bolted together and the oven door closed. The oven is switched on and set to 200°C. The temperature in the oven is checked continuously and when it passes 146°C the oven is set at that temperature and allowed to reach equilibrium. The equilibrium is determined when the temperature reaches $146^{\circ}C \pm 1^{\circ}$. In the meantime temperature readings are frequently made for the two internal tanks as well as for the water tank. The temperature of the water is adjusted until the equilibrium of the whole system is achieved at $62^{\circ}C \pm 0.1^{\circ}$.

The beaker around the flask is filled with water and the hot plate underneath is turned on. This procedure will bring the water to boil before the liquid polymer is introduced. The measuring of the two components is now begun. Valve 4 Figure 3.7, is opened and the liquid flows into the antechamber, when the latter is 3/4 full, valve 4 is closed and valve 3 is opened. This introduces nitrogen pressure above the liquid in the antechamber and drives the liquid into the buret. Valve 3 is closed and valve 6, Figure 3.8, is opened which removes the nitrogen through the vacuum system. The burets are only partially filled and therefore this process is repeated until they are completely full. When the burets overflow the vacuum is left on. by leaving valve 6 open, until all the bubbles in the buret are drawn off. Now valve 6 is closed and valve 3 opened again introducing nitrogen pressure over

the liquid in the burets. Valve 8 is opened and the excess liquid is removed from the antechamber. Now valve 7 is opened and the liquid from the burets flows into the mixing flask. As soon as the mixing is begun a timing clock is started; also the mechanical stirrer is switched on. When the burets have emptied, valve 11 is opened and the flask is evacuated. After three minutes of mixing the stirrer is switched off and the valve 11 is left open for an additional one minute to remove all the bubbles from the mixture. Also at the same time valve 9 is opened and this evacuates the mold. Valve 11 is now closed and 12 is opened. This introduces nitrogen pressure over the mixture and it is driven into the preheated mold.

The liquid polymer is cured in the mold for one hour at 146°C. After this time the oven is switched off and the door opened. The mold is now unbolted into its two halves and the sheet of the solid polymer removed. The material is now labled and placed in a dry box for storage. The material is left to age for at least five days before being used for experimental specimens.

Each casting uses only a very small portion of the components in the preheating tanks and therefore these tanks are used for storing this material between castings. During such time a slight nitrogen pressure is maintained over the components to prevent any leakage of air from outside.

As mentioned previously there are two sizes of the Solithane 113 material which are presently being case; one is circular 14 inches in diameter and one-tenth of an inch thick, the other is six inches by six inches square and one-half inch thick. However, there is very little limitation on a possibility of casting other shapes and sizes if they are desired. Only an appropriate mold has to be constructed and the sizes of the measuring burets changed.

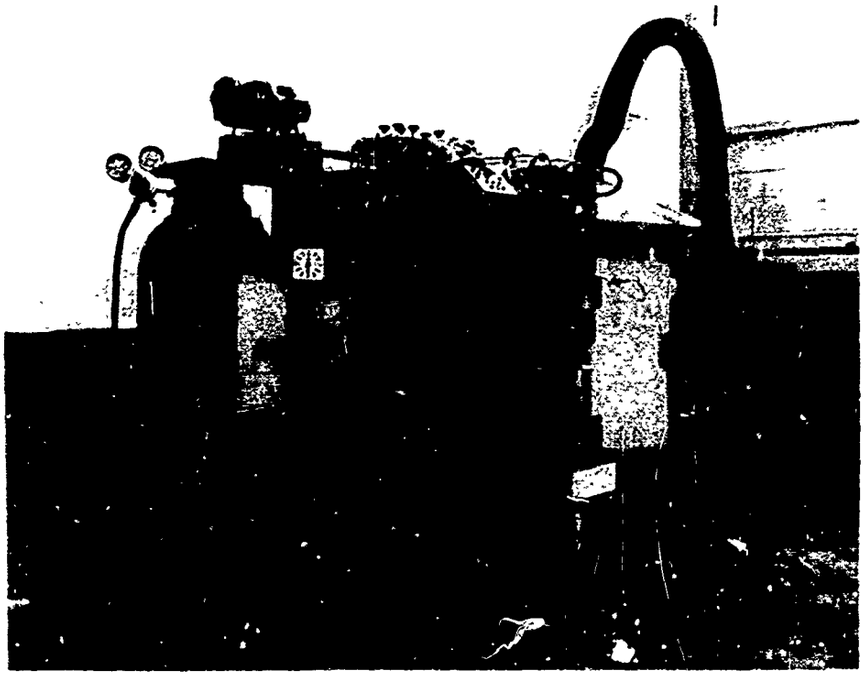

Fig. 3.1. The Overall View of the Solithane 113 Manufacturing Facility.

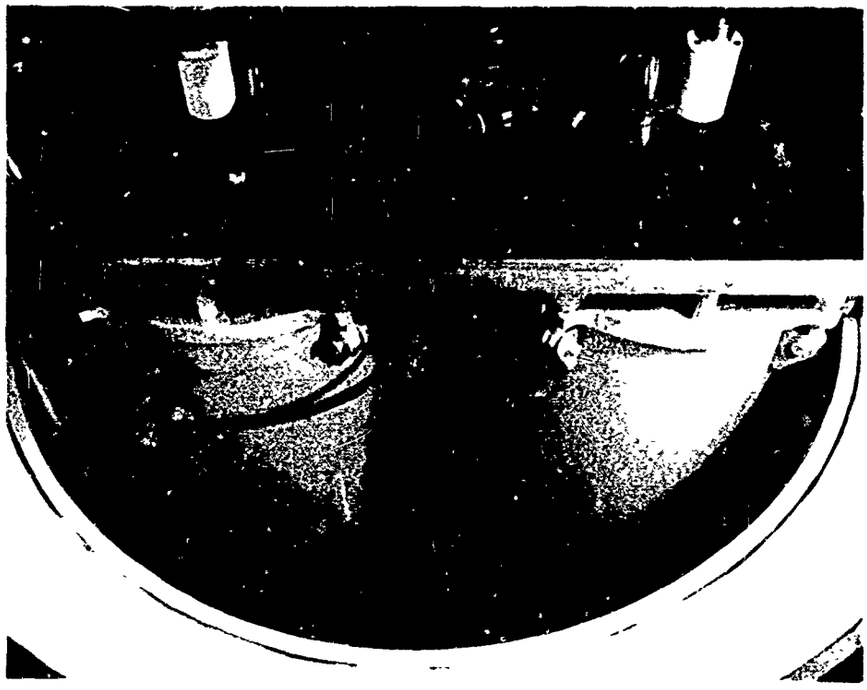

Fig. 3.2. The Preheating and Storing Tanks for the Prepolymer and the Catalyst.

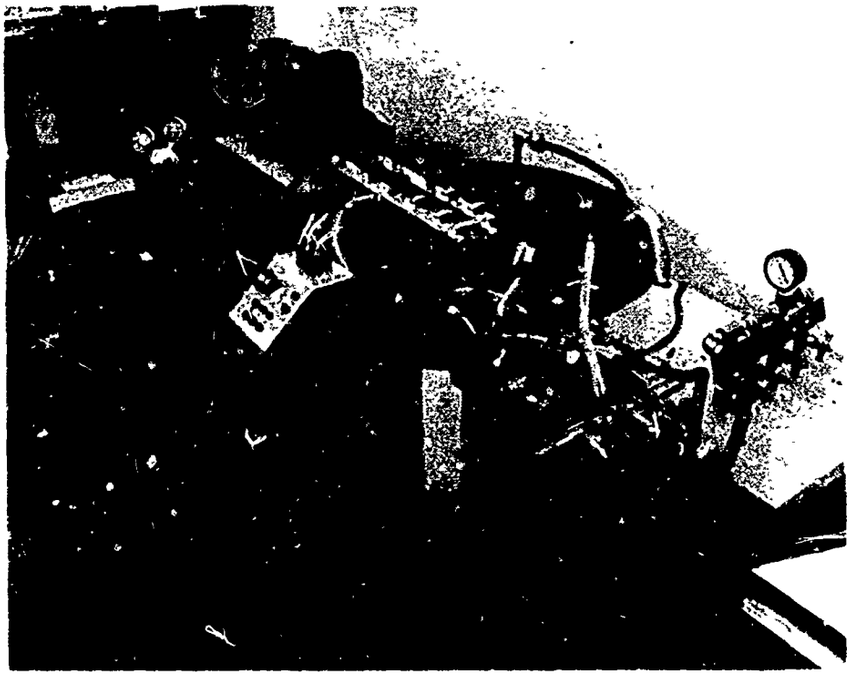

Fig. 3.3. Top View of the Casting Facility Showing the Control Valves and the General Arrangement.

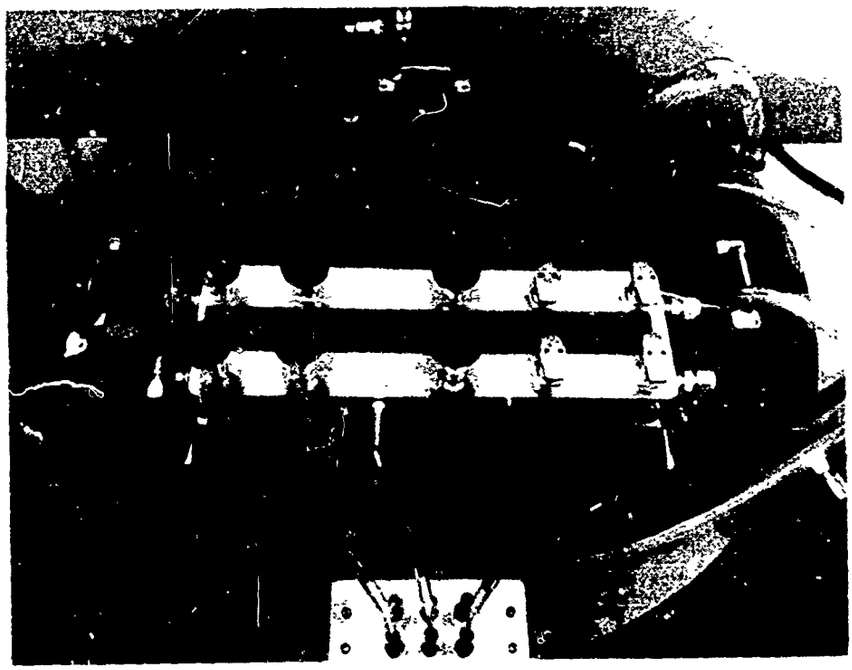

Fig. 3.4. Top View of the Water Tank Showing the Control Valves and the Belt and Pulley Arrangement for the Stirring Mechanism.

Fig. 3.5. Measuring Burets and the Mixing Flask.

Fig. 3.6. Curing Oven and the Circular Mold.

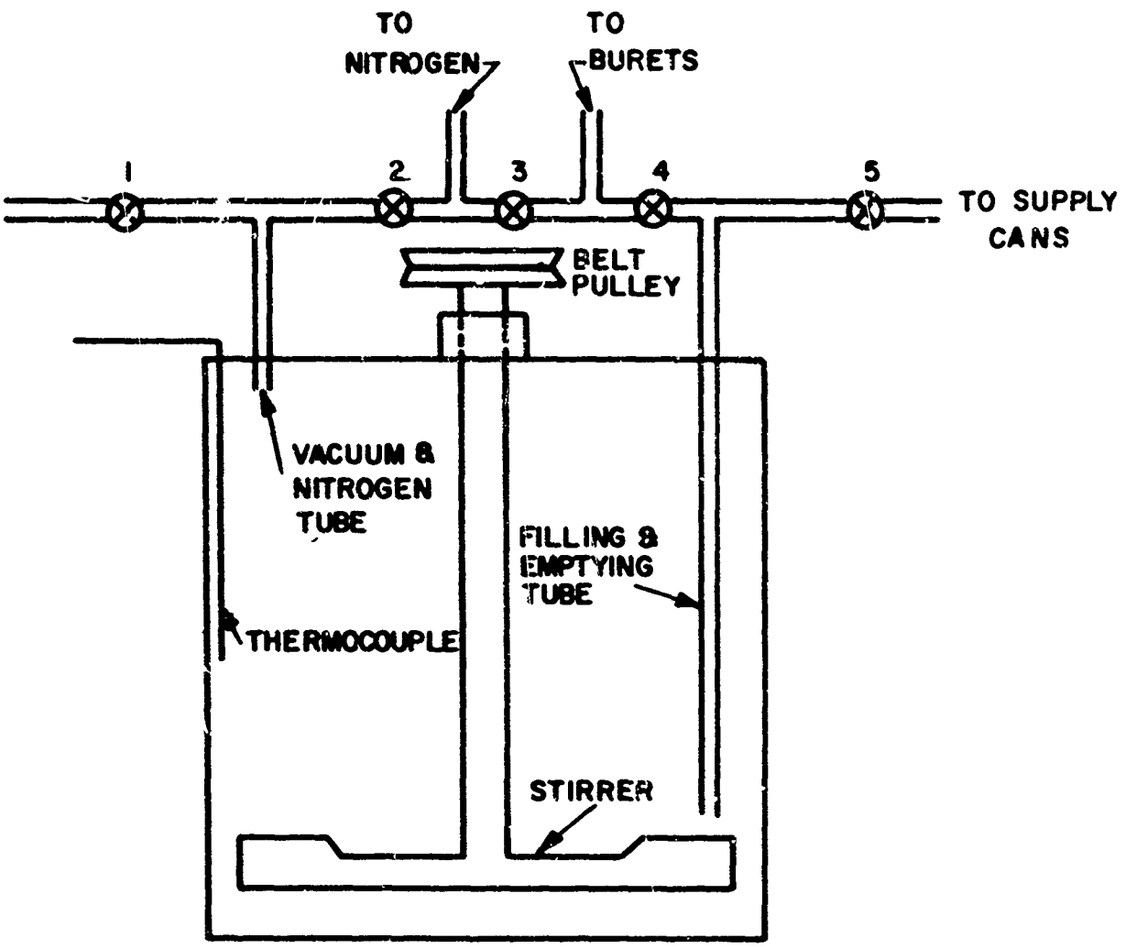

Fig. 3.7. Schematic Arrangement of the Prepolymer and the Catalyst Tanks.

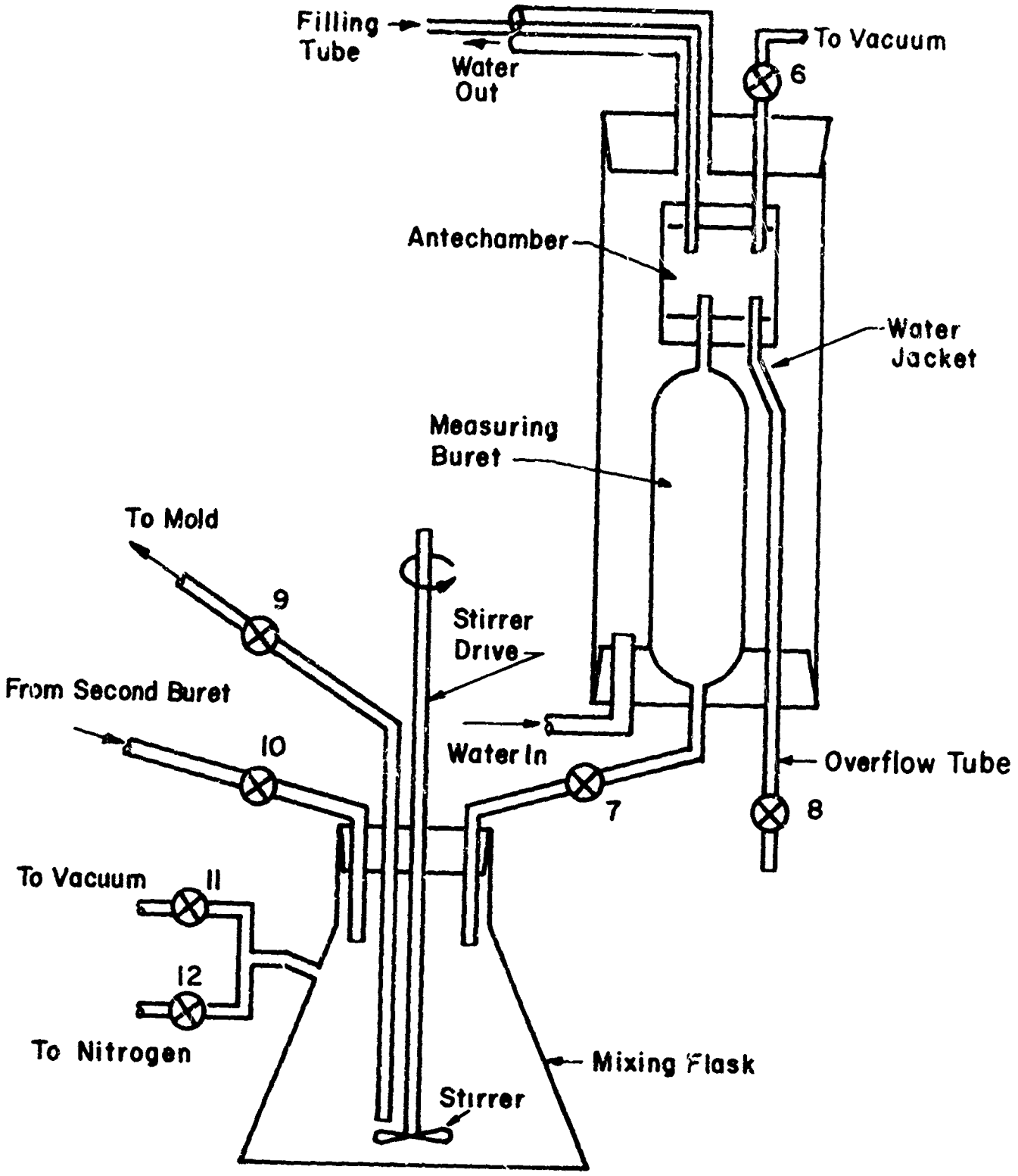

Fig. 3.8. Schematic Arrangement of the Measuring Buret and the Mixing Flask.

4.0 EXPERIMENTAL PROGRAM

4.1 INTRODUCTION

The purpose of the experimental program, which is at present in progress, is two fold. First, it is required to obtain viscoelastic characterization of the mechanical properties of the Solithane 113 material. Such a characterization is necessary so that viscoelastic stress analyses can be carried out for this material. The necessity of such a stress analysis was illustrated in the previous section in the case of the "poker-chip" specimen. The second purpose of this experimental program is to obtain failure data for the Solithane 113 material under various stress conditions. It is hoped to use the results of these tests to check out the failure theory developed and described earlier in this report. We shall now describe these two phases of the experimental program.

4.2 MATERIAL CHARACTERIZATION

4.2.1 Description of Solithane 113 Material

Solithane 113 is a urethane type polymer for which the components are produced and sold by the Thiokol Chemical Corporation. Chemically the urethane polymers are the product of a reaction between an isocyanate and a hydroxyl:

$$-N=C=O \quad + \quad H-O- \longrightarrow -\underset{\underset{H}{|}}{N}-\underset{\underset{O}{|}}{C}-O$$

isocyanate + hydroxyl ⟶ urethane

Because the isocyanates are basically toxic and react easily with hydroxyl groups the base for the Solithane 113 is made and sold in a form of a prepolymer. These prepolymers are stable at room temperature and therefore nontoxic. They are prepared by combining the isocyanates with certain groups so that the product is still reactive at elevated temperatures. Solithane 113 is made from this prepolymer by addition of a catalyst and curing at elevated temperatures. In our program the Thiokol catalyst C 113-300 is used for this purpose.

The Solithane 113 can be made with widely different mechanical properties by varying the relative amounts of the prepolymer and the catalyst. The ratio which is used in the present program is one to one by volume. Before a decision was made to use this mixture various other ratios were tried. A larger proportion of the prepolymer to catalyst, 10 to 7, produced a rather hard material which was not very suitable for investigation of the viscoelastic effort. Going to the other extreme a ratio of prepolymer to catalyst of 7 to 10 was tried. This produced a rather soft material with a very low tear resistance. Preliminary failure studies in uniaxial tension were conducted with this material and it was found that the results were very sensitive to surface imperfections. Therefore, this material was not considered to be suitable for the failure investigations.

4.2.2 Quality Control Tests

In the last section the Solithane 113 manufacturing facility was described and it was emphasized that this facility was designed and built to provide a high degree of process control. Therefore, the first tests that were conducted on the new material were aimed at establishing whether indeed the control on the manufacturing process was sufficiently close as to produce uniform mechanical properties from batch to batch. For this purpose a uniaxial test was chosen. From each of seven different batches of the material a uniaxial specimen was milled. The dimensions of this specimen are shown in Figure 4.1. The uniaxial load to the specimen was applied at each end through two thin strips of aluminum which were bonded on both sides of the specimen over one-half inch of its length. The bond was made with Eastman 910 Adhesive. The aluminum strips overlapped the specimen and a metal spacer was placed between them. The specimen was then placed in an Instron testing machine by being gripped on the aluminum strips. This arrangement is shown in Figure 4.1. The test consisted of subjecting each specimen to a constant strain rate by applying a cross-head extension rate of 0.2 inches per minute. The load on the specimen was recorded as a function of time and since the rate was constant, also as a function of the extension. Each specimen was loaded to fracture. It was desired to compare the variations of the load with time for each specimen.

The load-time curves for each of the seven specimens were found to lay within the two curves shown in Figure 4. 2. The maximum variation is approximately five percent from the mean. This order of magnitude agreement was considered to be an indication of sufficient reliability and control in the manufacturing process of the material.

Although the specimens were loaded to fracture it was not intended to obtain failure data from these tests. The breaking point occurred in the vicinity of the bonded ends of the specimen where the stress field was not uniform and the fracture was obviously affected by the discontinuous conditions caused by the bonded aluminum strips.

4. 2. 3 Relaxation Modulus Characterization

As indicated in Section 2 the knowledge of the relaxation modulus for a material is necessary in order that a viscoelastic stress analysis may be carried out. Therefore, a set of uniaxial tests have been designed and are presently being conducted in order to obtain this information for the Solithane 113 material. The overall dimensions of the specimen used in these tests are shown in Figure 4. 3. The specimens are milled from the one-tenth of an inch thick sheet stock. The shape of the specimen was chosen after a preliminary investigation of a number of alternate configurations. The choice was made on the basis of preliminary tests to failure. It is intended to use the same specimen for the uniaxial failure data as well as for obtaining the viscoelastic characterization. It is therefore, important that the specimen configuration chosen for this study be such that the failure occur in the region of uniform, uniaxial stress field. In the particular configuration shown in Figure 4. 3 this does indeed happen, it is found that the failure occurs in the two inch center portion of the specimen. The stress field in this region has been observed to be quite uniform.

The tests are conducted in an Instron testing machine. The specimens are gripped at each end through bonded aluminum strips, this arrangement is very similar to that used on the quality control tests described in the previous section. The dimensions and the arrangement of the gripping strips are shown in Figure 4. 3. In the tests the specimens are subject to constant strain conditions. These conditions are obtained by applying a constant rate of movement to the bottom crosshead. Such a constant movement applies a nearly constant extension rate across the two inch center portion of the

specimen. The relation between the movement of the crosshead and the strain in the specimen is shown in Figure 4. 4. This relation was obtained by a preliminary test where the strain on the one and one-half inch center portion of the specimen was measured directly using a traveling microscope and was compared to the machine extension. Also in this test the strain was measured directly over one-half inch center portion of the specimen. The strains obtained by using the 1-1/2 inch and the 1/2 inch gage lengths are compared in Figure 4. 5. The results of this comparison show that the strain over the two inch center section is quite uniform.

The tests are being conducted at different constant strain rates and at different temperatures. The temperature environmental conditions are supplied by a Missimers temperature box which is specially constructed for use with the Instron tester. This facility provides cold as well as hot conditions relative to room temperature. As mentioned before, each test is conducted to failure. The data is recorded on the Instron strip chart in the form of load versus time and, since the strain rate in each test is constant, this also gives the strain information.

The data obtained from these tests will be used to generate the relaxation modulus for the Solithane 113 material. The relationship between the constant strain rate response and the relaxation modulus is quite simple and can be derived as follows. For a linear viscoelastic material the stress-strain law can be written in an integral form

$$\sigma(t) = \int_0^t E(t-\tau)\ \frac{d\epsilon}{d\tau}\ d\tau \qquad (4.2.1)$$

where σ is the stress, $E(t)$ is the relaxation modulus, ϵ the strain and, t the time. For constant strain rate conditions

$$\epsilon = R\ t \qquad (4.2.2)$$

where R is the strain rate. Substituting from equation (4. 2. 2) to (4. 2. 1) we have

$$\sigma(t) = \int_0^t E(t-\tau)\ R d\tau \qquad (4.2.3)$$

Making an independent variable substitution under the integral sign of equation (4. 2. 3)

$$x = t - \tau \tag{4. 2. 4}$$

we have

$$\sigma(t) = R \int_0^t E(x)\, dx \tag{4. 2. 5}$$

From equation (4. 2. 5) it follows that

$$\frac{1}{R} \frac{d\sigma(t)}{dt} = E(t) \tag{4. 2. 6}$$

Equation (4. 2. 6) shows that the relaxation modulus for a linear viscoelastic material is equal to the time rate of change of stress divided by the strain rate in a constant strain rate test. This relationship will be used to evaluate the relaxation modulus from the data of the constant strain rate tests.

In order to fully characterize the relaxation modulus it is necessary to carry out the constant strain rate test over a wide range of temperatures and strain rates. At present these tests are being conducted and so far data has been obtained at two temperatures; at 27°C and 35°C. At each of these temperatures tests have been carried out at four different strain rates corresponding to the Instron crosshead rate motion of . 02, . 2, 2. 0 and, 20 inches per minute. In order to insure the repeatability of results three tests have been conducted at each temperature and strain rate. The data obtained in these tests can only define a small portion of the relaxation modulus. Consequently the tests are being continued and extended to other temperatures. The data obtained so far will not be discussed at this time and the complete set of data will be presented at a later date at which time the relaxation modulus will be evaluated.

4.3 FAILURE TESTS

As mentioned before, it is intended to perform three different failure tests on the Solithane 113 material. In these tests the material will be subjected to failure under uniaxial, biaxial and the triaxial stress conditions. These tests are to be conducted over a wide range of strain rates and temperatures. The purpose of these tests is to accumulate basic strength data on the material and to use this data to check out the multiaxial failure theory which was developed and presented in Section 1.0 of this report.

The uniaxial failure data is being obtained from constant strain rate tests simultaneously with the data for the relaxation modulus characterization. These tests have been described in Section 4.2.3. This group of tests is now in progress and the failure data which has already been obtained will be presented. The biaxial tests, which have not as yet been started, will be of a strip-type. This test has been explained in detail in Section 1.5.2 of the previous Interim Report[4.1]*. In the strip biaxial test the material is subjected to an unequal biaxial stress and plane strain condition. Certain preliminary configurations of this test have already been investigated for the new Solithane 113 material. The specimens have been milled from the cast one-tenth inch thick sheets of the material. The tests on this configuration will begin after the completion of the present uniaxial testing program. The results will be presented in the subsequent reports.

In this program the failure under the triaxial tension field is being obtained by the use of the poker-chip specimen. This type of a test has been explained in detail in Section 2.0 of the previous Interim Report[4.1]. A set of triaxial experiments has been completed using the new Solithane 113 material. These have been conducted at various strain rates and temperatures. The results of these tests will be presented and discussed.

4.3.1 Uniaxial Failure Data

Since the uniaxial failure tests are being conducted simultaneously with the characterization tests therefore, the failure data has now been obtained for the two temperatures, 27°C and 35°C, and the four strain rates

---

* Superscript refers to references at the end of the section.

described in Section 4. 2. 3. Just as in the case of the relaxation modulus characterization, these tests are not sufficient to completely define the uniaxial failure. The full set of data will be available when the uniaxial tests have been completed and the detailed discussion and analysis of this data will be presented at the later date. However, in order to illustrate the repeatability of the present tests the data obtained so far is presented in Figures 4. 6 and 4. 7. Figure 4. 6 shows the ultimate load as a function of the strain rate in the center portion of the specimen. The corresponding ultimate extension ratio is shown in Figure 4. 7. The results indicate a definite effect of temperature and strain rate. The scatter in the data obtained from the different tests under same temperature and strain rate is considered to be small. It was observed during the tests that the failure in all cases has occurred within the one and one-half inch center portion of the specimen.

4. 3. 2 Triaxial Poker-Chip Tests

The configuration of the poker-chip test was described in detail in Section 2 of the previous Interim Report[4. 1]. Since that time this test has been modified and considerably improved. The complete poker-chip assembly, which is presently being used, is shown in the photograph of Figure 4. 8. By comparing this set-up to the previous one, which is shown in Figure 2. 1 of reference 4. 1, two main differences are immediately apparent. First, the steel holders into which the Lucite extensions screw in have been changed. The new holders had to be built in order to reduce bending in the poker-chip specimen. Because of its flat geometry the specimen was found to be extremely sensitive to any misalignment in the holders and the Lucite extension rods. The previous components were made with standard machine shop tolerances and this was found to be not accurate enough with the result that appreciable bending was present in the specimen during the tests. Therefore, present holders, seen in Figure 4. 8, were designed and built. Special machining procedures were used in obtaining close tolerances. Since the alignment of the threads on the Lucite extensions is equally important, new extensions were machined with the same tolerances as used in the holders. As a result of these new and more accurate components

the bending in the specimen was reduced appreciably. For example, the average maximum bending strain, calculated from over fifty different tests, is now only 11 percent of the average strain. This is a substantial improvement.

The second obvious change which can be seen in Figure 4.8 is in the displacement transducers which measure the extension of the specimen. The transducers used in the previous set-up can be seen in Figure 2.1 of reference 4.1. The new transducers are linear-variable-transformer coils made and sold by Shaevitz Engineering. Their sensitivity is at least an order of magnitude greater than that of the previous transducers. Consequently the extension readings for the specimen are now much more accurate. There are two of these transducers and they are mounted diametrically opposite each other across the poker-chip specimen as can be seen in Figure 4.8. Each transducer sits inside a specially constructed holder, which allows for very accurate axial movement of the transducer core. Such an arrangement is necessary to insure accurate readings. The transducers can be operated at low as well as high temperatures.

The readings of the two transducers are recorded simultaneously on a Mosley dual-pen X-Y recorder. The recorder can be seen in the photograph of Figure 4.9. The two extensions readings are plotted against time. The load on the specimen is recorded on the Instron strip recorder also as a function of time. The electrical input into the transducers is produced by the two small boxes which can be seen sitting on the top of the Mosley recorder in Figure 4.9. These boxes also demodulate the output of the transducers to a direct current signal.

The bonding procedure for attaching the poker-chip specimen to the Lucite extension rods has also been improved. The procedure now is as follows: the ends of the Lucite rods to which the specimen is to be attached are sanded down with aluminum oxide paper and then they are cleaned with methyl alcohol. A two inch square piece of Solithane is cut from the sheet stock and cleaned with methyl alcohol. The Solithane is placed on a flat metal surface and Eastman 910 Adhesive accelerator is applied to the top side and is allowed to dry. The 910 Adhesive is now applied to one of the Lucite rods and the rod is now placed in contact with the Solithane. In order to exclude any air bubbles between the Solithane and the Lucite rod the rod is first held at some small angle to the specimen and the initial contact is made at one point

only. Then the rod is gradually rotated until full contact is made. This motion spreads the adhesive uniformly across the interface. The bond is allowed to dry for five minutes. The accelerator is now applied to the other side of the specimen and allowed to dry. The Lucite ex ension rod to which the Solithane has already been bonded is now placed in a bottom portion of a V-shape jig with the unbonded face of the specimen facing up. The 910 Adhesive is now applied on the second rod and it is allowed to flow to one edge of the bonding surface. Therefore, the adhesive is thicker at this point than at any other. This Lucite rod is now placed in the top portion of the jig and it is brought down slowly on top of the specimen. Because of the uneven distribution of the adhesive the first contact is made at only one point and as the extension is brought down further the adhesive is spread evenly over the interface without formation of any air bubbles. The Solithane material is now trimmed to a circular, two inch diameter specimen.

The V-shape jig is used in order that the two Lucite extension rods may be accurately aligned with each other. Any misalignment would cause bending. The new procedure of bonding which has just been described, is much faster and produces more consistent bonding strength than the approach used previously.

4.3.3 Triaxial Failure Data

A set of the poker-chip triaxial failure tests has now been completed and the results will be presented in this section. The tests have been run at six different temperatures varying from -10°C to 45°C. The tests were conducted at each temperature at two different strain rates, these correspond to the .02 and the 0.2 inches per minute extension rates of the Instron testing machine. At each temperature and the crosshead extension rate, at least three different specimens were tested. Some data was eventually rejected because of obvious bond failure. It was not possible to test at higher rates of extension above 0.2 inches per minute since this produced a very high strain rate in the specimen and the time to fracture at these higher rates was found to be extremely short. Consequently it was not possible to record this data on the present recording equipment.

The failure data obtained in these tests is presented in Figures 4.10 and 4.11. Figure 4.10 shows average breaking stress, calculated by dividing the total axial load by the specimen cross-sectional area, as a function of the average axial strain rate. The average strain rate was calculated from the two displacement measurements across the specimen. As mentioned previously, these displacements have been recorded as a function of time on the Mosley plotter. The corresponding average ultimate extension of the specimen is shown as a function of the average strain rate, in Figure 4.11.

It can be seen from Figures 4.10 and 4.11 that there exists an appreciable scatter in experimental results. However, the results definitely indicate the affect of the strain rate and temperature. In order to illustrate more clearly these effects a straight curve was drawn through the data for each temperature. These curves suggest that a WLF shift function could possibly be applicable to both the average ultimate stress and the average ultimate strain data. However, since the curves are to some degree arbitrary, because of the scatter in the data, there will be no attempt to shift them at this time. A possible shift function of the Solithane 113 material will first be investigated in the case of the uniaxial data which is presently being obtained. As mentioned before, the uniaxial data which has been obtained so far does seem to be much more reproducible and therefore it is expected that a shift function investigation on this data will be much more conclusive. If an existence of a shift function is established in this way the triaxial failure data in Figure 4.10 and 4.11 will then be shifted.

The reason for the large scatter in the failure data in these tests has not yet been determined. The scatter is definitely not produced by faulty bonding since after each test the fracture has been examined closely to determine whether it reached the Lucite-Solithane interface. If this happened the test data was disregarded and not included in Figures 4.10 and 4.11. Eventually it is intended to conduct more poker-chip tests in which it is hoped that some of the reasons for the scatter may be determined.

Before the present data can be compared with the failure theory developed in Section 1.0 it is necessary that a viscoelastic analysis of the poker-chip specimen, described in Section 2.0, be completed. For the

lack of the viscoelastic characterization of the Solithane 113 this analysis can not be completed at this time. Therefore, the comparison of the failure theory and the experimental data will be carried out at a later date.

REFERENCES

4.1 Lindsey, et al.,: "The Triaxial Tension Failure of Viscoelastic Materials," ARL 63-152, Aerospace Research Laboratories, United States Air Force, September 1963.

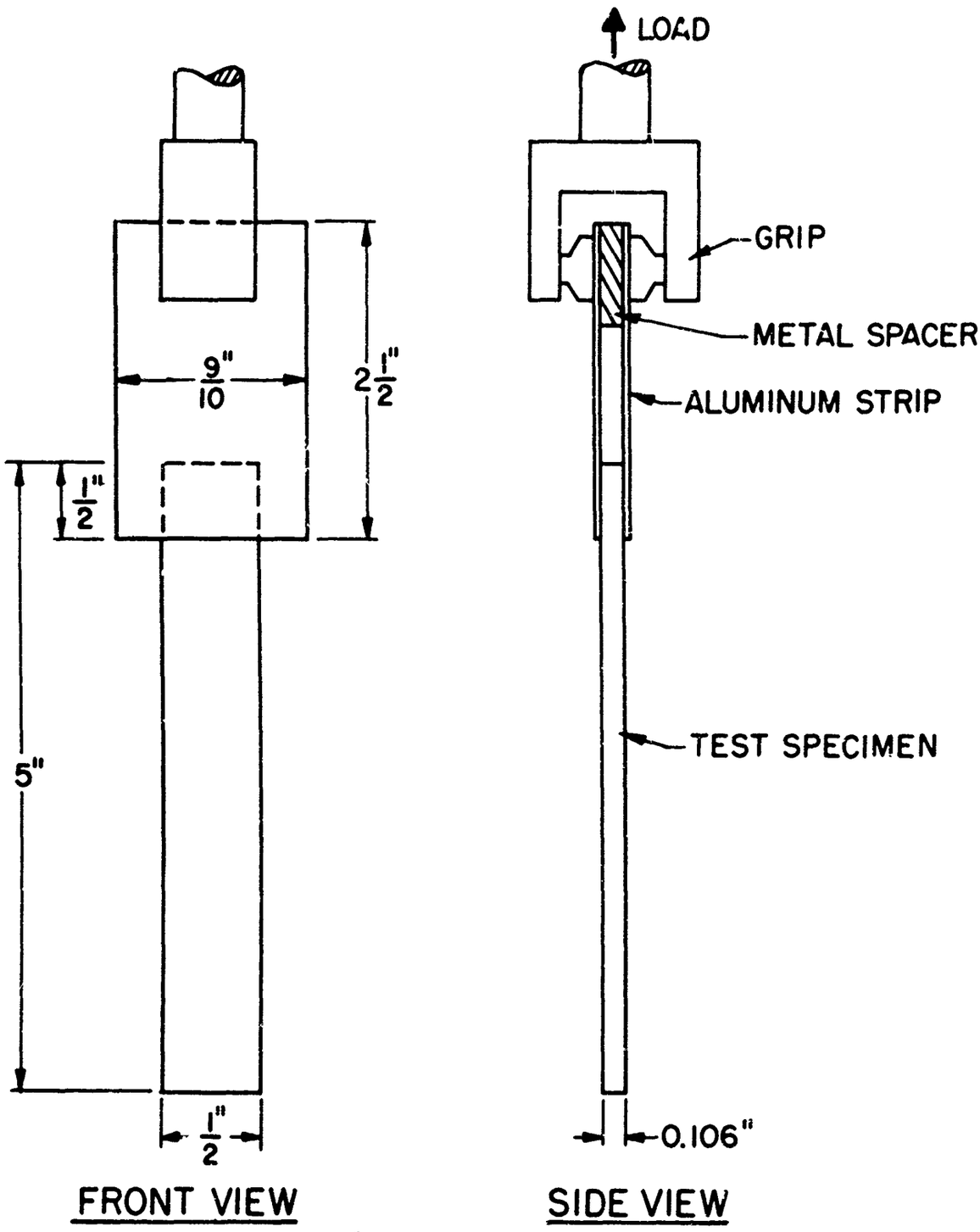

Fig. 4.1 Dimensions and the Attachment of a Uniaxial Specimen Used for the Mechanical Properties Reproducibility Tests.

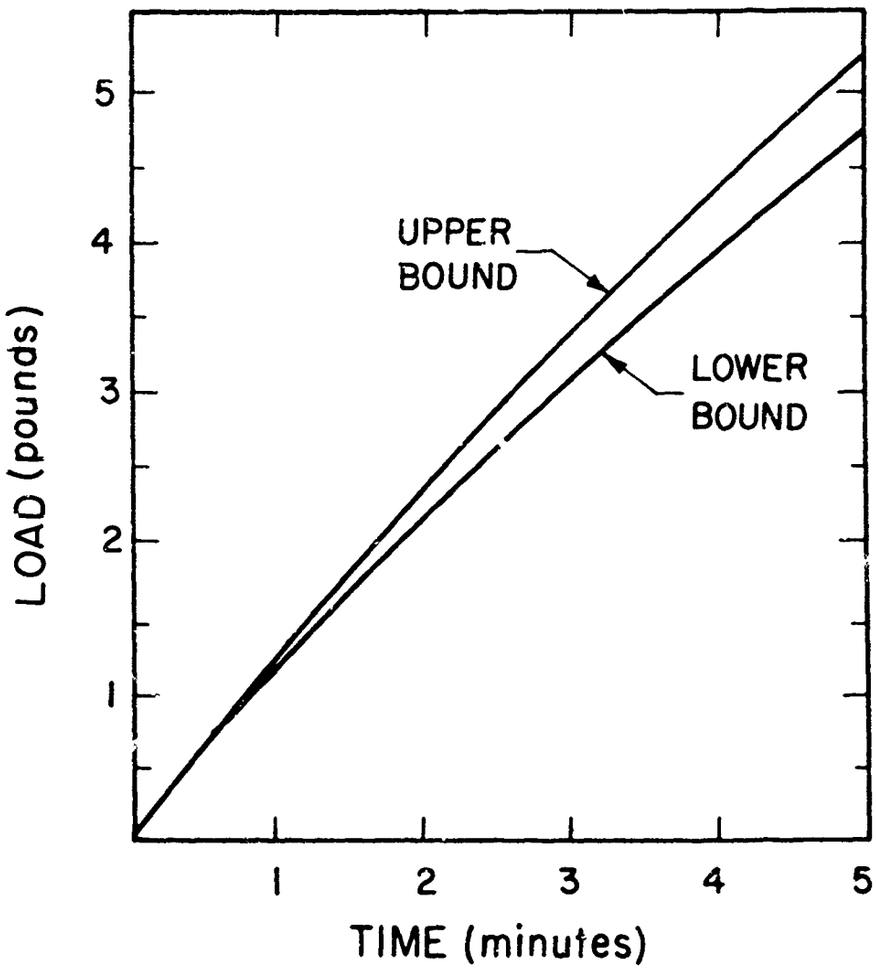

Fig. 4.2 Upper and Lower Bounds on the Load-Time Curves Obtained from Seven Different Uniaxial Specimens.

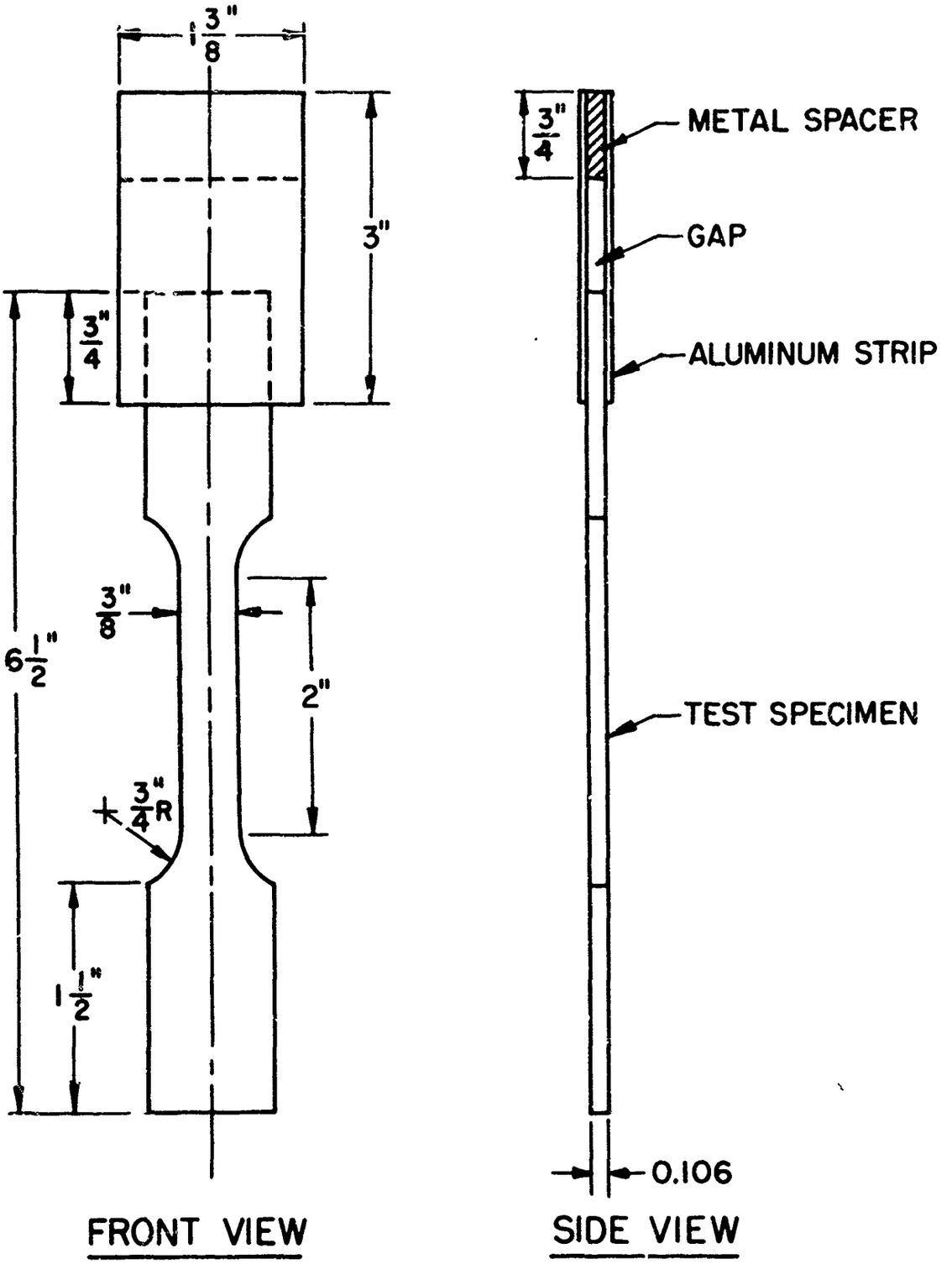

Fig. 4.3 Dimensions and the Attachment of the Uniaxial Specimen Used for the Viscoelastic Characterization and the Uniaxial Failure Properties Tests.

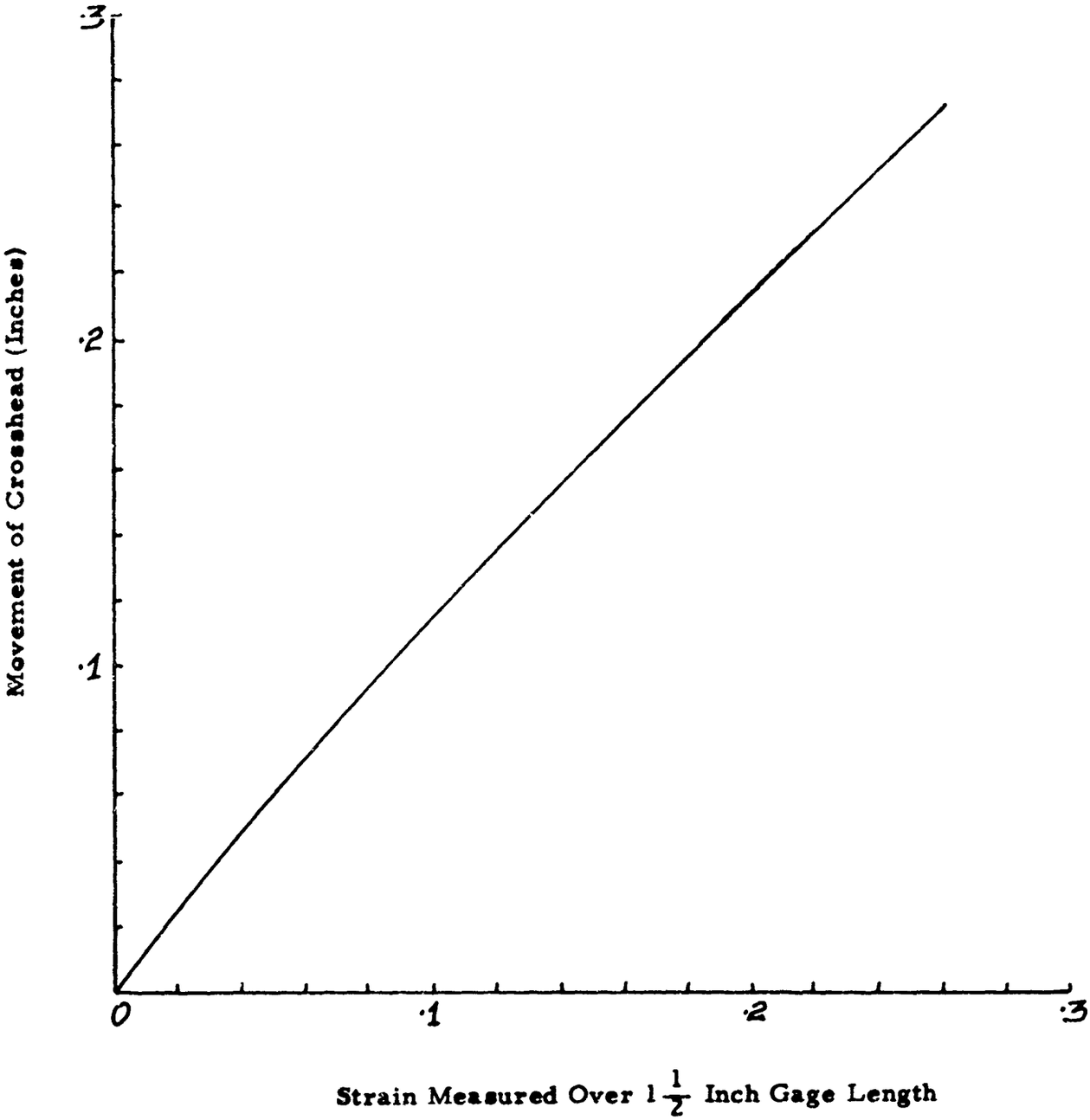

Fig. 4.4 Comparison of the Crosshead Movement of the Instron Machine With the Strain Measured Optically Over the Center Portion of the Uniaxial Specimen.

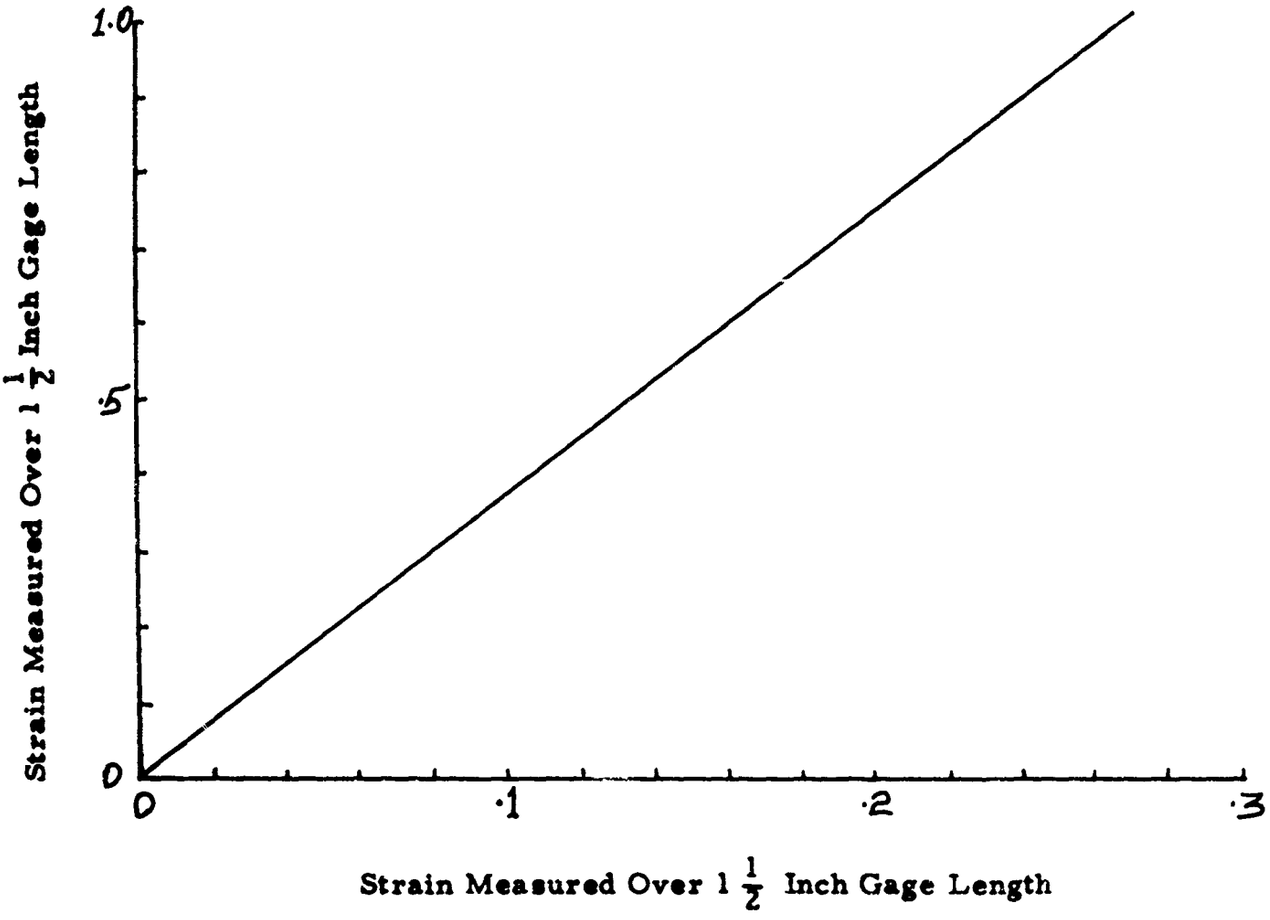

Fig. 4.5 Comparison of Strains Measured Optically Over Two Different Gage Lengths in the Center Portion of the Uniaxial Specimen.

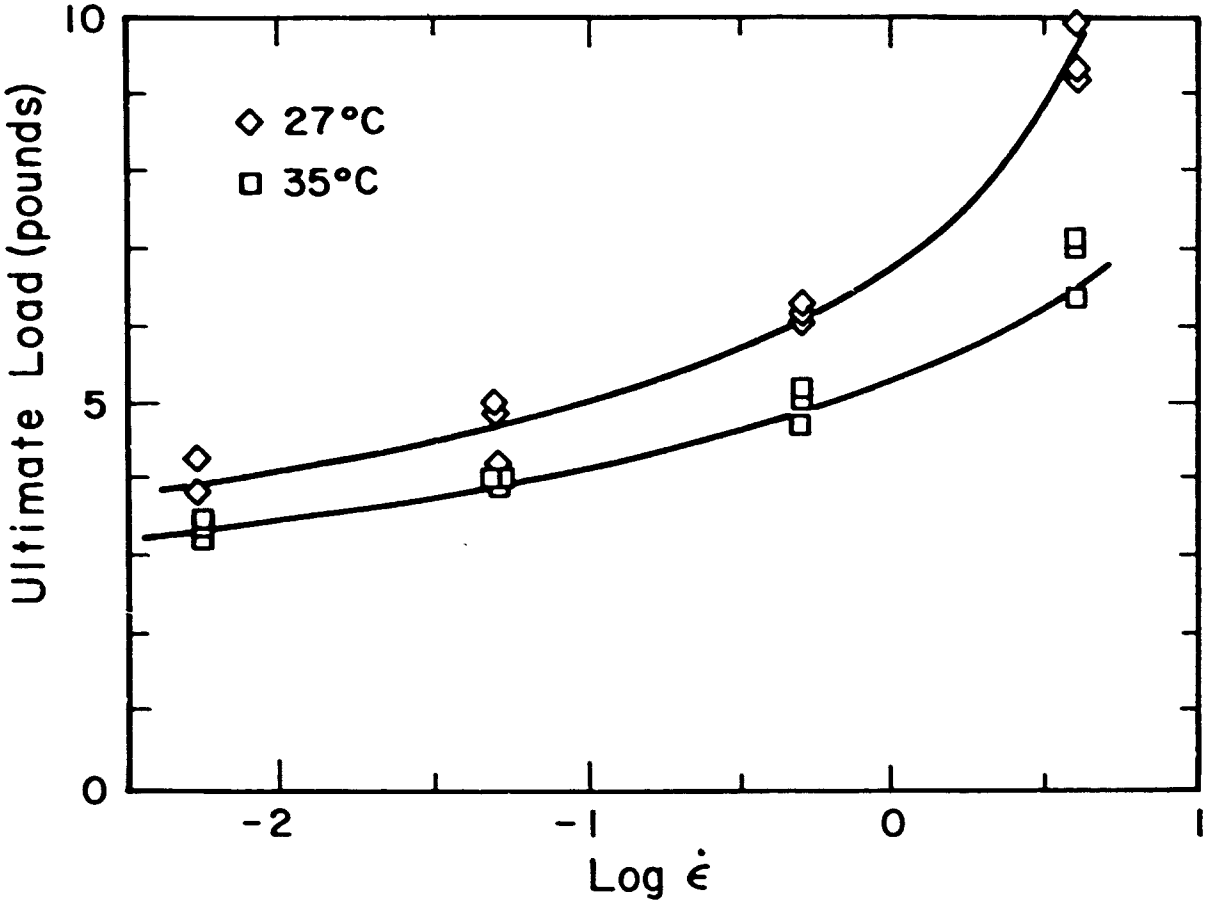

Fig. 4.6. Dependence of the Ultimate Load in the Uniaxial Test on the Strain Rate $\dot{\epsilon}$ for Solithane 113 Material at Two Different Temperatures.

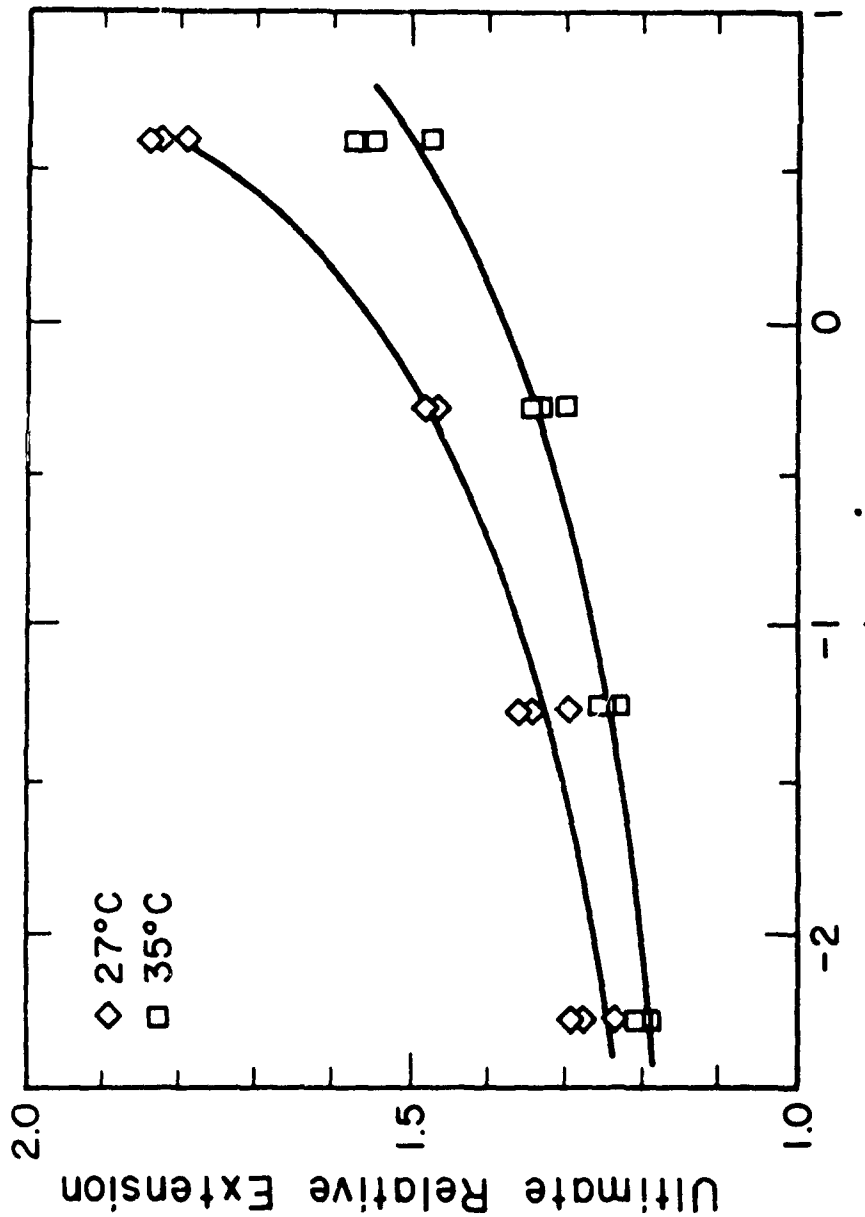

Fig. 4.7. Dependence of the Ultimate Relative Extension in the Uniaxial Test on the Strain Rate $\dot{\epsilon}$ for Solithane 113 Material at Two Different Temperatures.

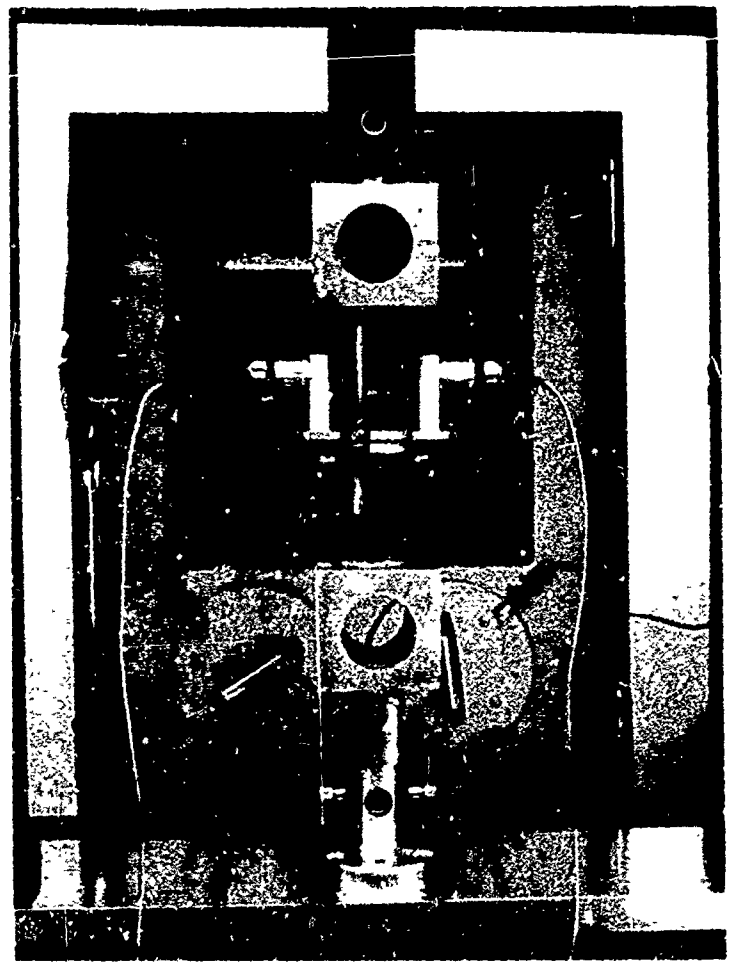

Fig. 4.8. Arrangement of the Triaxial Test.

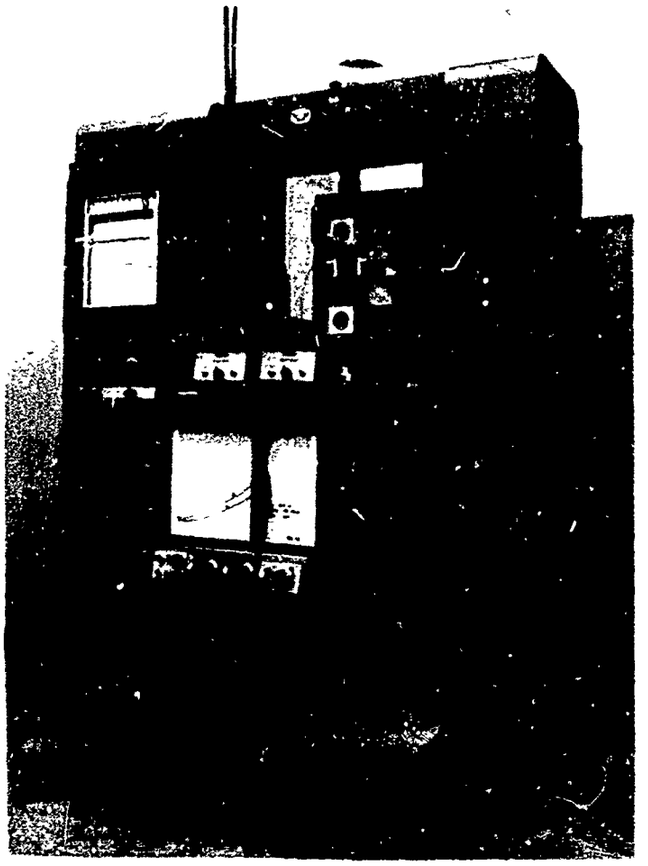

Fig. 4.9. General View of the Triaxial Test Showing the Specimens in the Instron Testing Machine and the Recording Equipment.

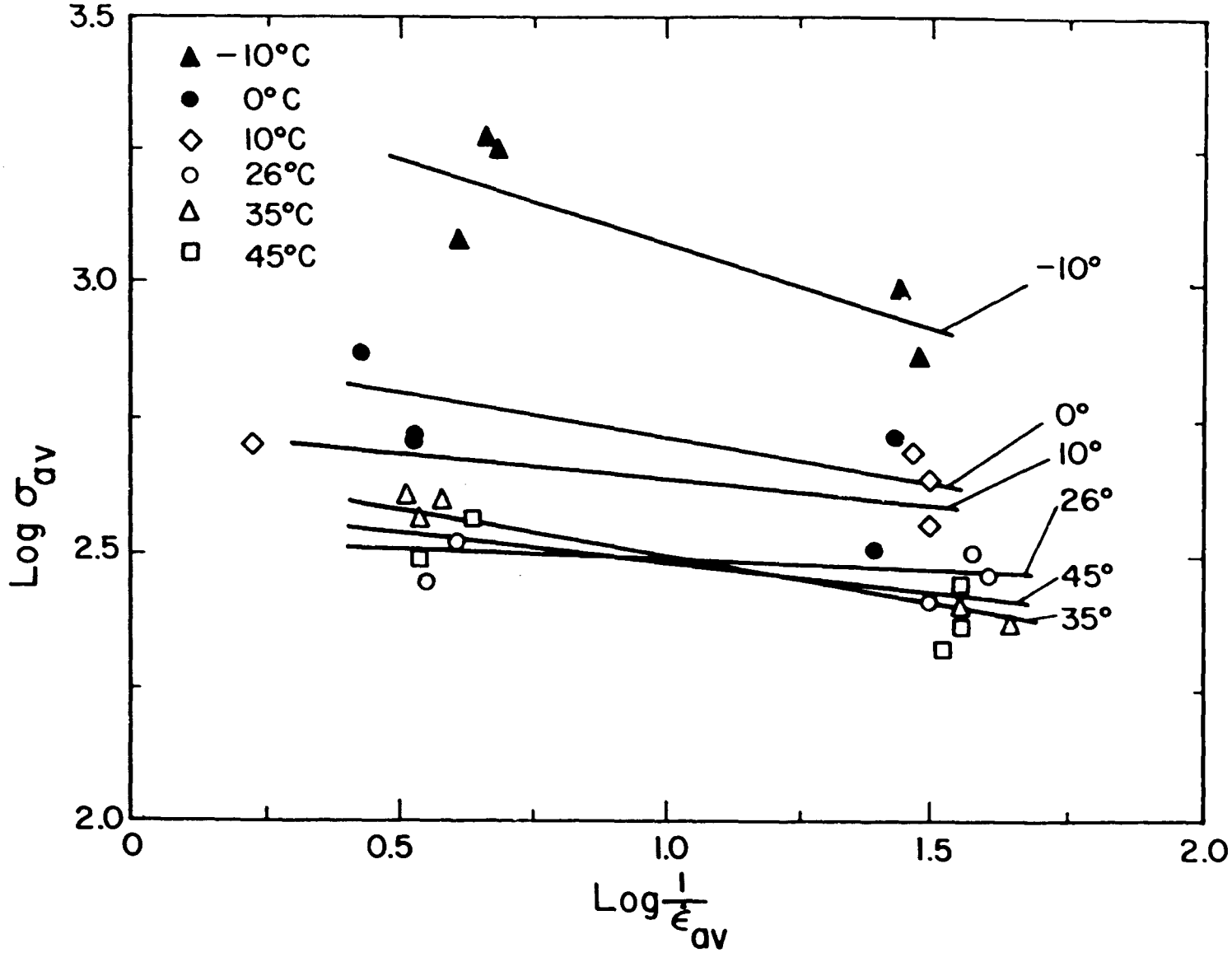

Fig. 4.10. The Dependence of the Average Stress σ_{av} at Failure on the Average Strain Rate $\dot{\epsilon}_{av}$ for the Solithane 113 Material in a Triaxial Test at Various Temperatures.

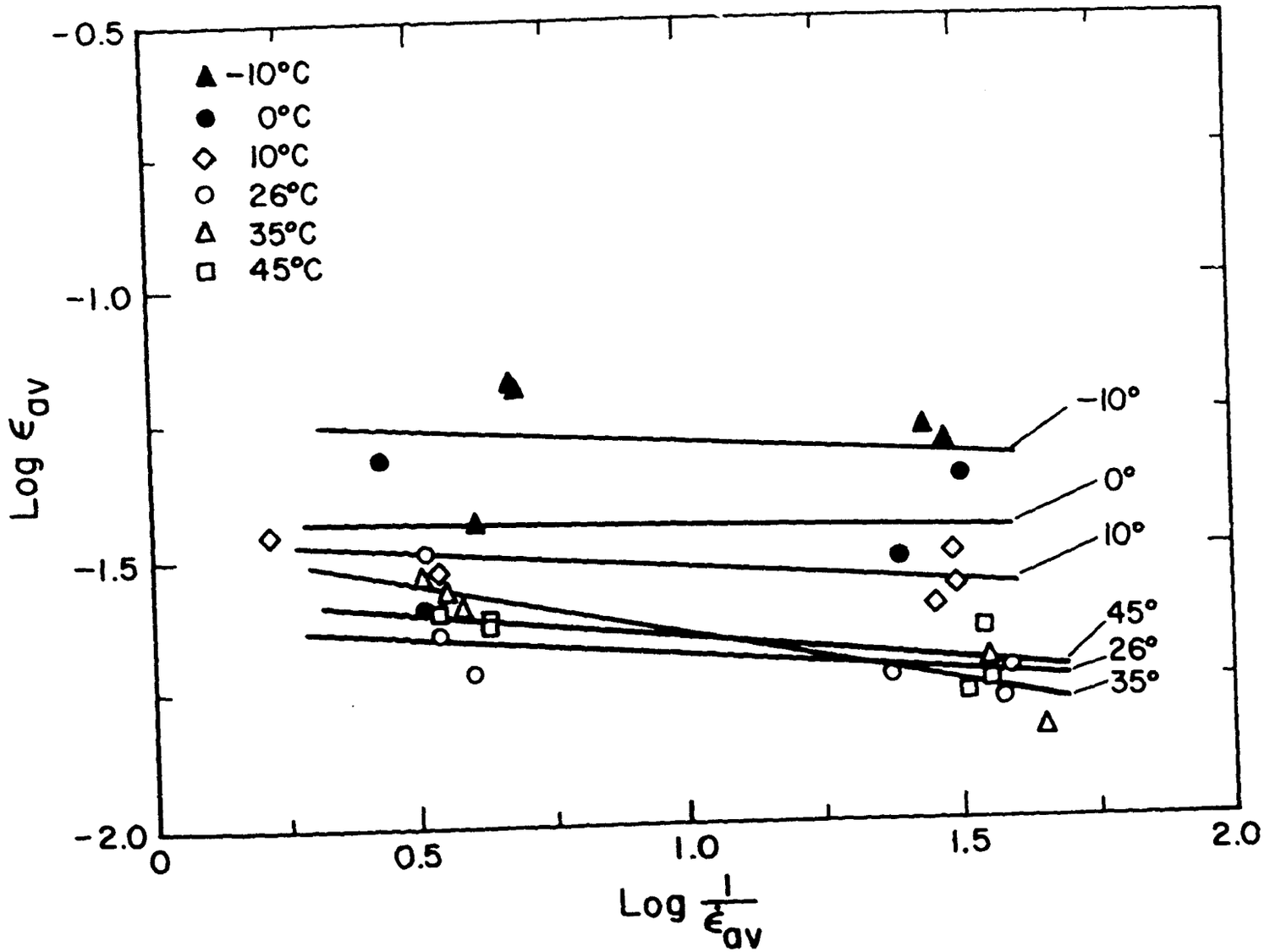

Fig. 4.11. The Dependence of the Average Strain ϵ_{av} at Failure on the Average Strain Rate $\dot{\epsilon}_{av}$ for the Solithane 113 Material in a Triaxial Test at Various Temperatures.